Modeling of Dry Deposition of SO_2 and Sulfate Aerosols

EA-1452
Research Project 1306-1

Final Report, July 1980
Work Completed, November 1979

Prepared by

AERONAUTICAL RESEARCH ASSOCIATES OF PRINCETON, INC.
50 Washington Road
P.O. Box 2229
Princeton, New Jersey 08540

Principal Investigators
W. S. Lewellen
Y. P. Sheng

Prepared for

Electric Power Research Institute
3412 Hillview Avenue
Palo Alto, California 94304

EPRI Project Manager
G. R. Hilst

Physical Factors Program
Energy Analysis and Environment Division

ORDERING INFORMATION

Requests for copies of this report should be directed to Research Reports Center (RRC), Box 50490, Palo Alto, CA 94303, (415) 965-4081. There is no charge for reports requested by EPRI member utilities and affiliates, contributing nonmembers, U.S. utility associations, U.S. government agencies (federal, state, and local), media, and foreign organizations with which EPRI has an information exchange agreement. On request, RRC will send a catalog of EPRI reports.

NOTICE

Prepared by
Aeronautical Research Associates of Princeton, Inc.
Princeton, New Jersey

ABSTRACT

A model for dry deposition of SO_2 and sulfate aerosol is presented. After a brief review of the literature, a model is formulated and calculations are made for four flow regimes: the outer boundary layer, the constant flux region, within the vegetative canopy, and the viscous sublayer next to a leaf or other smooth surface. The results of a number of calculations are presented to demonstrate the sensitivity of deposition to such variables as atmospheric stability, surface resistance, plant area density, plant structural shape, aerosol particle size, Rossby number, and canopy Reynolds number. A relatively simple parameterized model suitable for the SURE regional model is constructed. Recommendations are included for experiments to reduce remaining uncertainties.

EPRI PERSPECTIVE

PROJECT DESCRIPTION

This project is a theoretical evaluation of the properties of gases and particles and of atmospheric processes which control the dry deposition losses of pollutants to underlying surfaces. Advanced mathematical models of atmospheric turbulent transport of gases and particles have been constructed and validated against experimental measurements. These models are then systematically simplified and adapted for use in the SURE regional air quality model. The models are also used to design more accurate experimental measurements of dry deposition in terrain and vegetation conditions for which satisfactory data do not now exist.

PROJECT OBJECTIVES

The primary objective of the project is to provide a comprehensive understanding of the rates at which airborne pollutants are deposited on the earth's surface. The second objective is to translate this understanding into mathematical forms which can be incorporated into regional air quality models. The third objective, to be pursued after the first two objectives had been met, is an evaluation of experimental measurements required to correctly predict deposition losses. These data would be required in any future use of the models.

PROJECT RESULTS

This project has met all of its objectives with remarkable success. The general model of dry deposition processes has been validated for the case of a corn field canopy (the only complete data set available). The systematic simplification of this model has progressed to the point where a single equation correctly portrays the deposition transport within 10 percent of the more complex model's prediction. The stage is now set for a much more accurate and reliable dry deposition predictive scheme.

In order to realize this potential, however, model sensitivity analyses show that further field measurements are required to account for variability of dry

deposition over different surfaces and vegetative conditions. The existing experimental data do not, for the most part, contain the appropriate information necessary to predict dry deposition within the accuracy this work has shown is possible. The detailed design of such field measurements is being pursued as a sequel to this project.

G. R. Hilst, Project Manager
Physical Factors Program
Energy Analysis and Environment Division

CONTENTS

ILLUSTRATIONS

TABLES

NOMENCLATURE

A	measured plant area per unit volume
A_f	frontal plant area per unit volume
A_w	wetted plant area per unit volume
B	modeling constant equal to the neutral turbulent Prandtl number
C	mean species concentration
C_o	species concentration at the ground
$\tilde{C}_\ell$	layer-averaged mean species concentration
c_1	proportionality constant in Eq. 3-22
c_c	species diffusion coefficient
c_D, c_{D_h}	u_*^2/u^2, u_*^2/u_h^2
c_f	skin friction coefficient
c_p	profile drag coefficient
$\dot{c}$	source term in species equation
$\tilde{c}$	slip correction factor in Eq. 4-1
c_*	$-\overline{w'c'}\,\big|_o/u_*$
D	diffusivity
D_1, D_2	model constants
D_B	diffusivity of particles due to Brownian motion
D_f	skin friction drag
D_I	diffusivity of particles due to inertial impaction
D_p	profile drag
d	displacement thickness due to canopy
d_p	particle diameter
E	electric field
e	electronic charge
F_i	body force
f	Coriolis parameter $= 2\Omega \sin\phi$
g	gravitational acceleration
$\hat{H}$, H	shape parameters for canopy flow and deposition
h	canopy height
I	inertial impaction as shown in Eq. 4-5

K	von Karman's constant = $u_*/[z(\partial u/\partial z)]_0$ in the neutral surface layer
K_1	empirical constant in Eq. 3-23
K_2, K_3	empirical constants in Eq. 4-9
k	Boltzmann's constant
ℓ	layer height
L	Monin-Obukhov length = $-u_*^3 T_0/(Kg\ \overline{w'\theta'}\|_0)$
LAI	leaf area index
LA_WI	wetted leaf area index
N	number density of particles
n	coordinate perpendicular to the leaf surface or other smooth surface
n_e	number of units of electronic charge e
PAI	plant area index
p	mean pressure
$\dot{Q}$	source term in energy equation
q	square root of twice the turbulent kinetic energy
q_s	q associated with the smallest turbulent eddies
q_T	q associated with the main turbulent eddies
R_1, R_2, R_3, R_4	resistance to deposition in the four regions as shown in Figure 3-1
R_5	chemical or biological resistance at the leaf surface
R_a	aerodynamic resistance
R_b	viscous sublayer boundary layer resistance
R_d	total resistance to deposition
R_{Diff}	sublayer resistance to diffusion
R_g	gaseous resistance to deposition
R_{Imp}	sublayer resistance to particle inertial impaction
R_s	surface resistance to deposition
R_t	total resistance to deposition
Re	canopy Reynolds number = $\tilde{u}h/\nu$
Ro	Rossby number = u_g/fz_0
S^+	dimensionless particle stopping distance
Sc	Schmidt number = ν/D
t	time
u_{A_i}, u_{A_j}	aerosol velocity
u_g	geostrophic wind in the x direction
$\bar{u}$	mean velocity component in the x direction
$\tilde{u}$	$\bar{u}$ at z = 2h

u_i, u_j, u_k	Cartesian velocity components
u_ℓ	horizontal velocity at the edge of laminar sublayer
u_*	surface shear stress velocity = $(\nu/\rho)^{\frac{1}{2}}$
v_g	geostrophic wind in the y direction
$\bar{v}$	mean velocity in the y direction
$\tilde{v}$	$\bar{v}$ at $z = 2h$
v_d	deposition velocity = $-\overline{w'c'}\|_o/C(z)$
v_{d_h}	deposition velocity at the top of canopy
v_{d_s}	deposition velocity at the surface = $-\overline{w'c'}\|_o/C_o$
$\tilde{v}_{d_\ell}$	layer-averaged deposition velocity = $-\overline{w'c'}\|_o/\tilde{C}_\ell$
$\bar{w}$	mean vertical velocity
x, y	horizontal coordinates
x_1	function defined in Eq. 3-8
z	vertical coordinate
z_o	surface roughness height
z_{o_θ}	surface roughness height for heat
z_{o_c}	surface roughness height for species
z_i	inversion height
α	model constant
δ_{ij}	Kronecker delta
δ_s	thickness of laminar sublayer
δ_*	critical length scale for particle deposition through the sublayer above leaf surfaces
ε	effective turbulent eddy diffusivity
ε_{ijk}	alternating tensor
θ	potential temperature
θ_o	ground temperature
θ_*	$-\overline{w'\theta'}\|_o/u_*$
θ_ℓ	temperature at the edge of laminar sublayer
θ_s	surface temperature
κ	thermal conductivity
Λ	macroscale of turbulence model
μ	dynamic viscosity
ν	kinematic viscosity
ρ	density
ρ_A	density of aerosol
σ_u	standard deviation of longitudinal wind velocity

σ_w	standard deviation of vertical wind velocity
τ	surface shear stress
τ_v	relaxation time of particle
ϕ	Monin-Obukhov functions for the constant flux layer
ψ_1	function defined in Eq. 3-18
Ω	earth's rotation

Superscripts

-	denotes ensemble average
'	denotes fluctuation about the mean

SUMMARY

When airborne pollutants from multiple sources are transported over distances of hundreds and thousands of kilometers, a key process which determines their fate is deposition onto the earth's surface. Any regional air quality prediction system must account for these losses since they control the airborne concentrations produced by a quasi-equilibrium between continuous pollutant emissions and deposition losses. Despite numerous empirical attempts to parameterize dry deposition rates, a satisfactory prediction scheme does not yet exist.

As a first step toward improving the reliability of predictions of dry deposition losses of gases and aerosols, this project undertook the development of a generalized theoretical framework for the processes which control the turbulent transport of airborne materials to surface deposition sites. The comprehensive, second-order closure models of turbulent transport previously developed by A.R.A.P. have been modified for this purpose and have been validated against experimental measurements. This effort has been very successful and offers a quantum improvement in the understanding and quantification of dry deposition processes.

Because the general equations are much too cumbersome to be used directly in regional air quality models, a systematic, physically based simplification of the general model has been completed. This effort has produced a readily usable parameterized model which is still accurate to within 10 percent of the complex model predictions.

These developments, plus a sensitivity analysis of the model, have led to a recommended experimental procedure for further field measurements which will extend the model's applicability to terrain and vegetation types for which the required experimental data do not now exist. The design of these experiments is being pursued as a sequel to the work reported here.

Section 1

INTRODUCTION

The dry deposition of a pollutant over a regional area is very complex involving such diverse phenomena as turbulent transport of mass and momentum, aerosol dynamics, leaf chemistry, plant biology, and land use. Deposition velocities have been measured under conditions of limited control so that insufficient information is generally available to extrapolate the velocities to other field conditions. This is a report on a study to unravel the contribution of turbulent transport to the deposition process. The goal is to provide guidance to future field observation so that the accumulated data will have greater applicability to general field conditions.

The next section gives a brief literature review. The intent is not as much to review all that is known but rather to highlight some of the anomalies in predicted deposition velocities. This is followed by our analysis of deposition which emphasizes the role of turbulent transport while parameterizing the other major variables. A sensitivity study is carried out on our model to determine the most critical parameters. A number of uncertainties remain which require further experiments before they can be removed. Recommendations for these experiments are presented.

The primary use of dry deposition models is likely to be in regional studies such as SURE (1). Our fundamental model developed here is too complicated to fulfill this role, but a simple parameterization is proposed for this purpose.

Section 2

LITERATURE REVIEW

A number of reviews of sulfur deposition have been made. A recent historical review of SO_2 deposition studies was given by Chamberlain (2) and a recent review of the available data on deposition of SO_2 and sulfate aerosols, as well as for a number of different gases and particulates is given by McMahon and Denison (3). Numerical values of v_d for a wide variety of surfaces and species have been measured. However, the data can rarely be reliably extrapolated to general field conditions, due either to insufficient documentation of the ambient conditions for the experiment or to modeling deficiencies. Our aim in the present section is to highlight some of the uncertainties surrounding deposition values.

Gaseous and particulate removal rates from a polluted atmosphere to environmental surfaces historically have been reported as deposition velocities, v_d, defined as the flux to the surface $\overline{w'c'}|_o$ divided by the airborne concentration, C, i.e.,

$$v_d = -\overline{w'c'}|_o/C(z)$$

Since a concentration gradient is necessary to deliver a flux to the surface (except in the nominal case of simple gravitational settling of large particles), v_d is necessarily a function of the height at which the normalizing concentration is measured. Table 2-1 gives the estimated deposition velocities for a number of different surfaces as agreed upon at a workshop of the 1977 International Symposium on Sulfur in the Atmosphere (4). Definition heights are not given but generally assumed to be about 1 m.

The literature often deals with the resistance of the surface layer to deposition which is defined as the reciprocal of the deposition velocity,

$$R_d = v_d^{-1}$$

This concept has the advantage that it can conveniently be divided into the resistance of the various layers through which the pollutant must pass to reach the

Table 2-1

DEPOSITION VELOCITY ESTIMATES
[From 1977 International Symposium on Sulfur in the Atmosphere (4)]

Nature of Surface	$v_d(SO_2)$ (cm s^{-1}) Range	Typical
Vegetation		
grass ≈ 0.1 m height	0.1 - 0.8	0.5
crops ≈ 1 m height	0.2 - 1.5	0.7
forest ≈ 10 m height	0.2 - 2.0	?
Bare soil		
dry, pH > 7	0.3 - 1.0	0.8
dry, pH < 4	0.1 - 0.5	0.4
wet, pH > 7	0.3 - 1.0	0.8
wet, pH < 4	0.1 - 0.8	0.6
Water	0.2 - 1.5	0.7
Dry snow		0.1
Countryside	0.2 - 2.0	0.8
Cities	?	0.7

surface. In Table 2-2, Garland (5) summarizes the deposition velocity and the elemental surface resistance found for a number of different surfaces by a number of investigators and wherever possible divides the resistance into gaseous, R_g, and surface, R_s, contributions. Of course, the aerodynamic resistance to diffusion must vary strongly with wind speed and stability. This was fully recognized by Garland who also gave R_g for different heights. Table 2-3 shows the difference for three different surfaces.

It is equally clear that the surface resistance can be highly variable. Fowler (6) shows the diurnal variation in SO_2 deposition to wheat during both a period of rapid growth, Figure 2-1, and senescence, Figure 2-2. Figure 2-1 shows a peak in v_d during the middle of the day when photosynthesis should be at a maximum, while Figure 2-2 shows a peak at night. The first is attributed to the open stomata of the crop during growth and the second to nighttime dew. Although the dew appears

Table 2-2

THE RESULTS OF SEVERAL EXPERIMENTAL INVESTIGATIONS OF SO_2 DEPOSITION[a]

Surface	Method etc.	v_g cm/sec	R_g scm^{-1}	R_s scm^{-1}	Author
Water	Gradient, Lake Ontario	2.2	-	-	Whelpdale and Shaw (1974)
	Gradient, Reservoir	0.41	1.86	0.56	Garland (1977)
Calcareous soil	Laboratory, mass balance			0.24 - 0.39	Payrissat and Beilke (1975)
Acid soil	"			1.2 - 3.8	"
Calcareous soil	Gradient, field	1.2	0.83	0.1	Garland (1977)
Grass	Gradient, field				
	Summer	0.8		0.8	Shepherd (1974)
	Autumn	0.3		3.0	
"	$^{35}SO_2$ tracer, field	0.8			Owers and Powell (1974)
Short grass	Gradient, field	0.85	1.2	0.34	Garland (1977)
Medium grass	" "	0.89	0.46	0.66	"
"	Tracer, field	0.19	0.38	0.45	"
Cotton Sedgemoor	Gradient, field	0.7	-	-	Holland et al (1974)
Wheat	Gradient, field	0.74	0.5	1 - 2.5	Fowler (1976)
Wheat		0.44	0.28	2.0	Dannevik et al (1976)
Soybean		1.25	0.11	0.69	"
Pineforest (dry)	Tracer	0.1 - 0.6	0.1	1.5 - 5.0	Garland and Branson (1978)
"	" "	1.0			Belot et al (1976)

[a]From Garland (5).

Table 2-3

EXAMPLE OF CALCULATED VALUES
OF THE GAS-PHASE RESISTANCE

Surface and z_0 (m)	Wind speed at 100 m (ms^{-1})	Monin-Obukhov length, L (m)	u_* (ms^{-1})	$R_g(1)$ (scm^{-1})	$R_g(100)$ (scm^{-1})
Grass	3	∞	0.13	1.25	2.1
(0.01)		- 11	0.18	0.89	1.21
	10	∞	0.45	0.41	0.67
		- 215	0.49	0.38	0.57
		+ 630	0.41	0.44	0.77
Cereal crop	3	∞	0.18	0.87	1.5
(0.1)		- 27	0.25	0.66	0.93
	10	∞	0.59	0.32	0.50
		- 480	0.64	0.30	0.45
		+1700	0.57	0.33	0.54
				$R_g(5)$	
Forest	3	∞	0.27	0.26	0.54
(1.0)		- 85	0.36	0.20	0.43
	10	∞	0.89	0.11	0.24
		- 1500	0.93	0.10	0.22
			0.88	0.11	0.24

Unstable conditions (L negative) assume a heat flux of 50 W m^{-2} and stable conditions (L positive) assume a downward heat flux of 10 W m^{-2}. L = ∞ when conditions are neutral. In stable conditions at the lower wind speed, the surface is isolated from the 100 m level, preventing diffusion from this height and making resistances from 1 m unpredictable.

Source: Garland (5).

to have reduced the surface resistance during the early night hours, it does not appear to be effective during the early morning hours. Fowler suggests this is because the early morning dew is light enough that it could become saturated with SO_2. Figure 2-3, from Liss and Slater (7), shows that the resistance of SO_2 across an air-water interface increases sharply as the pH of the water decreases.

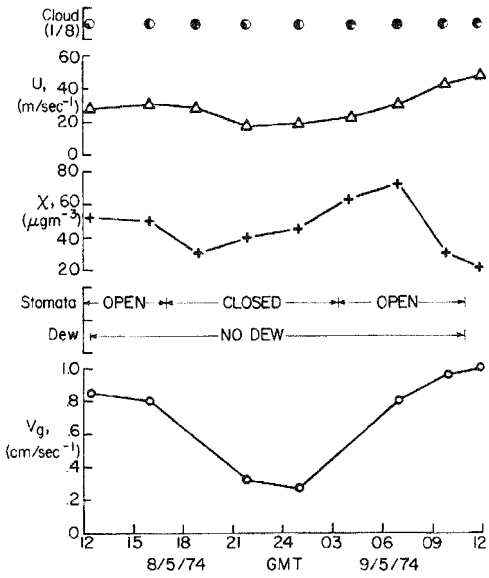

Figure 2-1. Dry deposition rates of SO_2 on wheat and other surface and atmospheric variables, during the period of rapid vegetative growth. [Source: Fowler (6)]

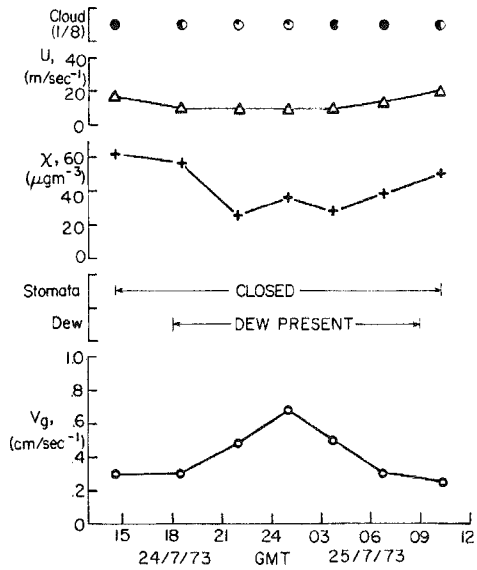

Figure 2-2. Dry deposition rates of SO_2 on wheat and other surface and atmospheric variables, during senescence of the crop. [Source: Fowler (6)]

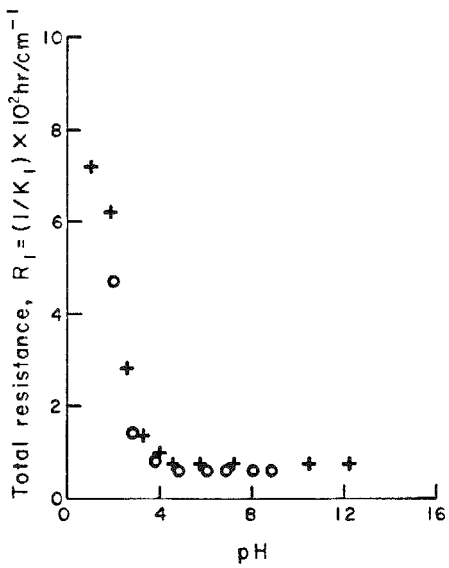

Figure 2-3. Variation of total resistance of SO_2 across an air-water interface with pH of the water. (o) Theoretical predictions of Liss. (+) Experimental results of Brimblecombe and Spedding. [Source: Liss and Slater (7)]

Fowler goes so far as to claim that dry deposition of SO_2 is usually controlled by the affinity of the surface for SO_2 rather than the conductivity of the atmosphere. However, this does not appear to agree with Garland's comparative resistances in Table 2-2. A consistent analysis of many of the factors affecting SO_2 deposition is given by Wesely and Hicks (8).

The status of estimating sulfate aerosol deposition is even more confusing than that for SO_2. The report from the International Symposium of Sulfur in the Atmosphere estimated that the deposition velocity for such aerosols was $\lesssim 0.1$ cm/sec. This seems to be based on the fact that particles of the size (0.1 - 1 μm diameter) containing most of the mass of sulfate aerosol are not transported efficiently across the laminar sublayer adjacent to a surface. This is shown in Figure 2-4, taken from Sehmel and Sutter (9). Estimates of low values have also been obtained from the field measurements of Droppo (10) and Lindberg et al. (11), but the most

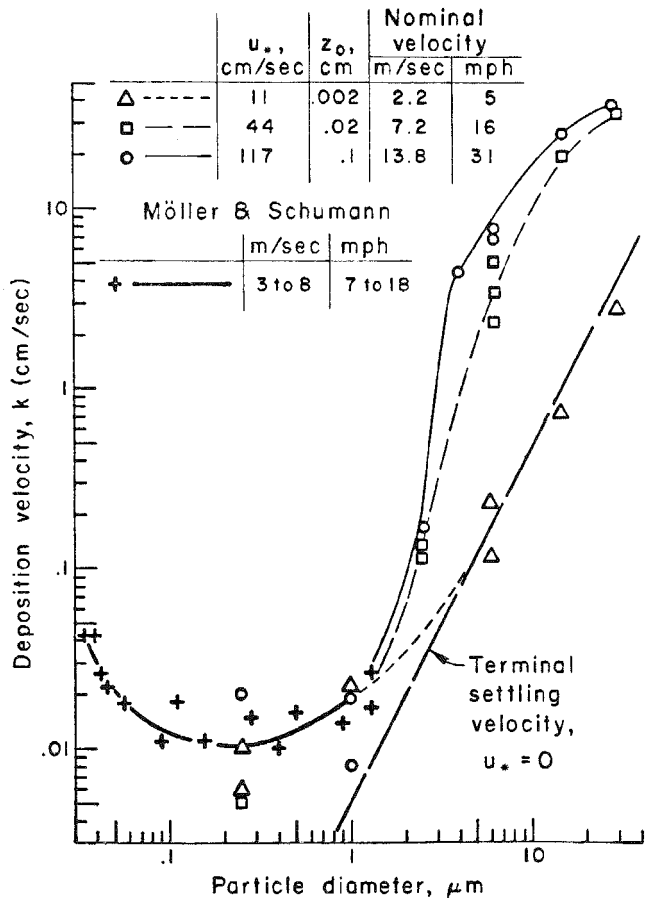

Figure 2-4. Deposition velocities to a water surface (particle density of 1.5 g/cm^3). [Source: Sehmel and Sutter (9)]

recent estimates made by Sheih, Wesely and Hicks (12) predict values as high as 1 cm/sec.

A number of the factors affecting the deposition of particles is given by Slinn (13). The most consistent available analysis of the dry deposition of small particles appears to be that by Sehmel and Hodgson (14). They correlated a number of different measurements to obtain an empirical relationship between the particle size and its resistance to transport across the viscous sublayer. This was combined with an analysis of diffusion in the constant flux layer similar to that to be discussed in the next section to obtain curves such as that reproduced here in Figure 2-5.

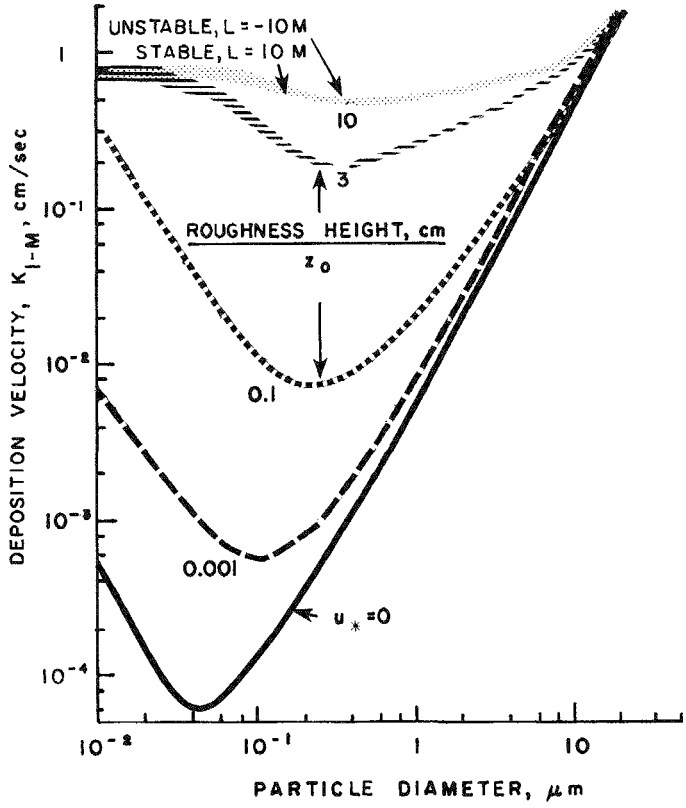

Figure 2-5. Predicted deposition velocities at 1 meter for u_* = 10 cm/sec. [Source: Sehmel and Hodgson (14)]

Note that there is some inconsistency between Figures 2-4 and 2-5. The Δ data points of Figure 2-4 which refer to u_* = 11 cm/sec, and z_o = 0.002 cm lead to

a minimum value of v_d ($\approx 10^{-2}$ cm/sec) about an order of magnitude higher than that indicated for the same conditions in Figure 2-5.

The recent paper by Sheih, Wesely and Hicks (12) presents estimates of surface deposition velocities of both SO_2 and sulfate particles over the eastern half of the United States, southern Ontario, and nearby oceanic regions for use in studies of regional scale atmospheric sulfur pollution. Based on land-use and likely biological status of vegetation during mid-summer conditions, average deposition velocities for grid cells corresponding to half-degree increments of longitude and latitude are presented for a range of atmospheric stabilities. The maps for neutral conditions are repeated in Figure 2-6. The most surprising thing about these figures is that over most of the land v_d is higher for sulfate (0.8 - 0.9 cm/sec) than it is for SO_2 ($\approx$0.3 cm/sec). This surprising result is a consequence of their assumption that the surface resistance to particle deposition is constant at 1.0 s cm^{-1}. It is also somewhat surprising that the only dependence on wind speed comes in the consideration of stability class.

The existence of such deposition maps should not be construed as an indication that all the questions surrounding deposition have been resolved. In fact, two of the same authors, Wesely and Hicks (15), have reported on measurements over a pine forest in Southeastern United States which show emission of small particles over most of the day with deposition only for a few hours near midday. From these measurements they conclude that further investigations are required to unravel surface deposition. The following sections represent our efforts to help in this endeavor. By constructing a model of turbulent transport to a vegetal canopy we hope to provide a framework for using the results of carefully controlled experiments to estimate deposition rates under general field conditions.

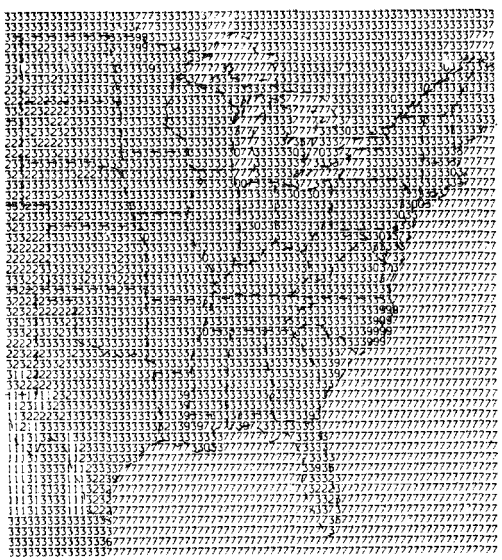

SO_2

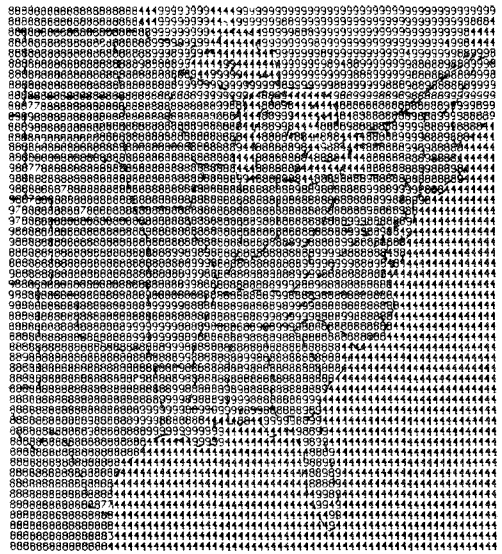

Sulfate

Figure 2-6. Map of deposition velocities of sulfur dioxide and sulfate particles for neutral stability. The alphanumerical symbols (0, 1, 2,..., 9, A, B,..., and F) in the map represent deposition velocity intervals of 0.1 cm s^{-1}; i.e., 0 and F represent the ranges of deposition velocities $0 < v < 0.1$ and $1.5 < v < 1.6$ cm s^{-1} respectively. [Source: Sheih, Wesely and Hicks (8)]

Section 3

DEPOSITION ANALYSIS

It is convenient to break up the boundary layer into four different regions as shown in Figure 3-1. The total resistance to deposition is the sum of resistance presented by each separate region plus a fifth resistance at the surface.

$$v_d = (R_1 + R_2 + R_3 + R_4 + R_5)^{-1} \qquad (3\text{-}1)$$

For flow over a smooth surface, region 3, the canopy, does not exist and $R_3 = 0$. When a vegetal canopy exists at the surface the effective surface area is increased, and R_4 is decreased and incorporated within R_3. A fifth resistance, a surface chemical or biological resistance, must be added to the four aerodynamic resistances in the most general case. Each of these layers will be considered separately.

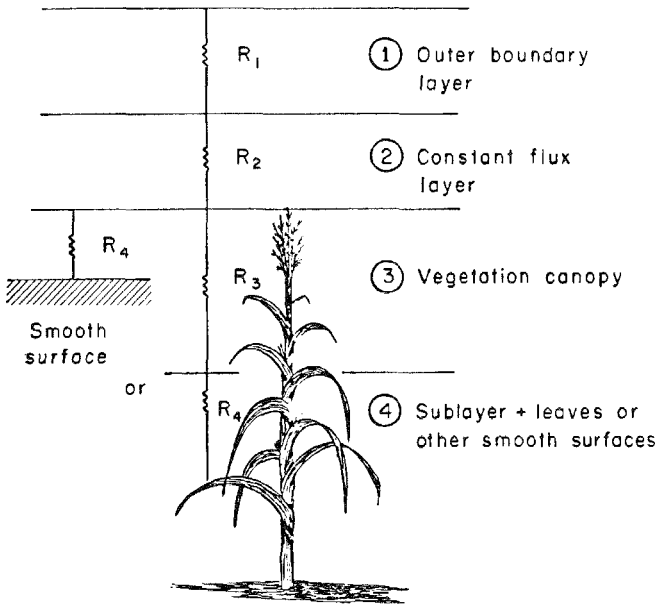

Figure 3-1. Four different regions of the planetary boundary layer for study of the aerodynamic resistance to SO_2 deposition.

OUTER BOUNDARY LAYER (Region 1)

The fundamental equation governing the species concentration in the outer boundary layer is

$$\frac{DC}{Dt} = -\frac{\partial \overline{w'c'}}{\partial z} - \frac{\partial \overline{v'c'}}{\partial y} - \frac{\partial \overline{u'c'}}{\partial x} \tag{3-2}$$

For regional scales the resulting distribution is essentially determined by a balance between vertical diffusion and horizontal advection, i.e., the equation can be approximated as

$$\frac{DC}{Dt} = -\frac{\partial \overline{w'c'}}{\partial z} \tag{3-3}$$

Our approach to solving this equation has been to couple it to the equation for $D\overline{w'c'}/Dt$ obtained by a careful modeling of certain terms in the exact equation derivable for $D\overline{w'c'}/Dt$. The fundamental assumptions of this approach were outlined by Donaldson (16). The solution for point and line source dispersal within the atmospheric boundary layer were given by Lewellen and Teske (17). The modeled equation for $D\overline{w'c'}/Dt$ is

$$\frac{D\overline{w'c'}}{Dt} = -\overline{w'w'}\frac{\partial C}{\partial z} + \frac{g}{T_o}\overline{c'\theta'} + 0.3\frac{\partial}{\partial z}\left(q\Lambda\frac{\partial \overline{w'c'}}{\partial z}\right) - \frac{0.75q}{\Lambda}\overline{w'c'} \tag{3-4}$$

The last two terms are the modeled terms representing turbulent diffusion and decorrelations terms. The second term on the r.h.s. of Eq. 3-4 is a buoyancy term which requires no modeling but couples in an additional equation derived in an analogous way.

$$\frac{D\overline{c'\theta'}}{Dt} = -\overline{w'\theta'}\frac{\partial C}{\partial z} - \overline{w'c'}\frac{\partial \theta}{\partial z} + 0.3\frac{\partial}{\partial z}\left(q\Lambda\frac{\partial \overline{c'\theta'}}{\partial z}\right) - \frac{0.45q}{\Lambda}\overline{c'\theta'} \tag{3-5}$$

Equations 3-3 to 3-5 form a complete set when the wind, temperature, and second-order velocity and temperature correlations are known or calculated from similarly modeled equations (11). When the surface and upper boundary conditions are spatially homogeneous, then the background wind and turbulence distributions may be taken to be functions of a single parameter, Rossby number = $u_g/z_o f$, provided the flow is neutral. Under stable temperature conditions, one stability parameter is required, say u_g/Lf; while for unstable conditions a second stability parameter, such as

z_i/L must be added. The surface, or top of the surface layer, condition on Eqs. 3-3 to 3-5 introduces one more parameter v_{d_h}/u_*. The deposition velocity is also a function of the height at which one chooses to define it.

In anticipation of using the deposition velocity in a regional scale model, it seems appropriate to define a layer averaged deposition velocity

$$\tilde{v}_{d_\ell} = - \overline{w'c'}|_o / \tilde{C}_\ell \tag{3-6}$$

with

$$\tilde{C}_\ell = \int_{z_o}^{\ell} uC\, dz \Big/ \int_{z_o}^{\ell} u\, dz \tag{3-7}$$

Based on the preceding argument, we expect $\tilde{v}_{d_\ell}/u_*$ to depend on the following dimensionless variables

$$\tilde{v}_{d_\ell}/u_* = \text{fcn.}\left(\frac{v_{d_h}}{u_*}, \frac{z_o}{\ell}, \ell/L, Ro, z_i/L\right) \tag{3-8}$$

or in terms of the resistance

$$R_1 u_* = \text{fcn.}\left(\frac{z_o}{\ell}, \ell/L, Ro, z_i/L\right) \tag{3-9}$$

The relative sensitivity of the different parameters will be explored in a later section.

CONSTANT FLUX REGION (Region 2)

The region of the boundary layer most amenable to simple analysis is the constant flux layer above any vegetative canopy and below advective contributions in the boundary layer. In this layer

$$\frac{Kz}{c_*}\frac{\partial C}{\partial z} = \phi(z/L) \tag{3-10}$$

This normalized species gradient is assumed to be the same function of z/L as the appropriately normalized temperature gradient. This assumption is based on the similarity of the fundamental heat and species diffusion equations, and there does not appear to be any reliable data which would refute this similarity. The function ϕ, shown in Figure 3-2, has been measured, e.g., (18) and predicted theoretically (19).

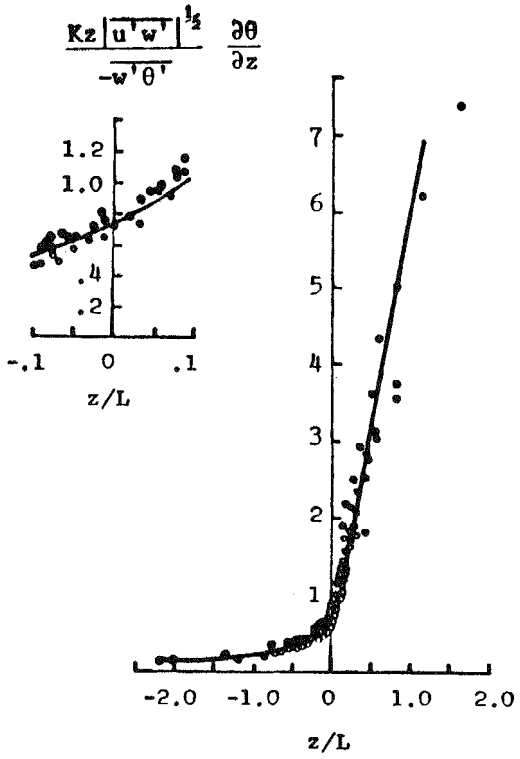

Figure 3.2a. Normalized velocity gradient as a function of the Monin-Obukhov similarity variable: model predictions, solid lines; observations (circles). [Source: Businger et al. (18)]

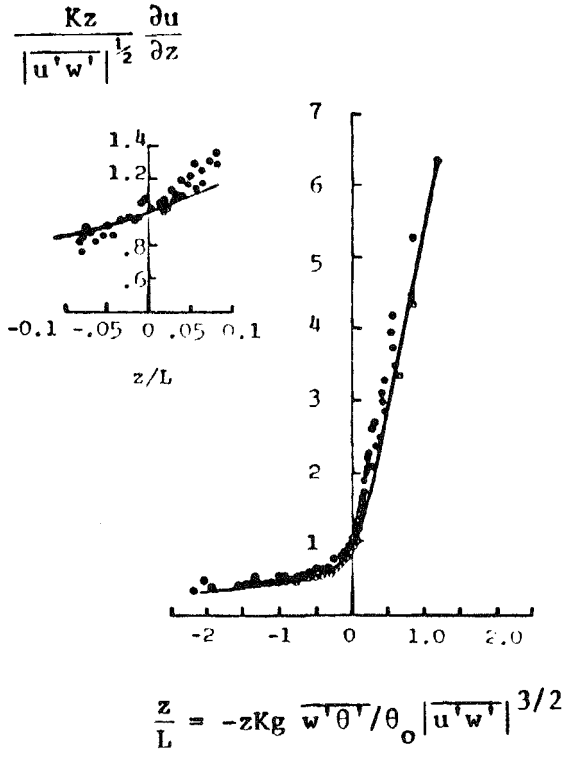

Figure 3.2b. Normalized temperature as a function of the Monin-Obukhov similarity variable: model predictions, solid lines; observations (circles). [Source: Businger et al. (18)]

Equation 3-10 can be integrated to obtain the species distribution

$$C - C_o = \frac{c_*}{K} \int_{z_{o_c}}^{z} \frac{\phi}{z}\, dz \qquad (3\text{-}11)$$

If we define surface resistance as the ratio of the surface concentration to the mass flux to the surface

$$R_s = - \frac{C_o}{\overline{w'c'}_o} \qquad (3\text{-}12)$$

Then Eq. 3-11 can be written as an equation for the deposition velocity at any height:

$$v_d(z) = \frac{-\overline{w'c'}|_o}{C(z)} \qquad (3\text{-}13)$$

i.e.,

$$\frac{u_*}{v_d} - u_* R_s = \frac{1}{K} \int_{z_{o_c}}^{z} \phi(z/L)\, \frac{dz}{z} \qquad (3\text{-}14)$$

Under neutral conditions ϕ = a constant $\equiv B\ (\approx 0.75)$ and a simple expression can be obtained for v_d

$$v_d = u_* \left[\frac{B}{K} \ell n\, z/z_{o_c} + u_* R_s \right]^{-1} \qquad (3\text{-}15)$$

Equation 3-14 can also be integrated for the full range of stability conditions from $-\infty \leq z/L \leq +\infty$, e.g., (20)

$$v_d = u_* \left[\frac{B}{K} \left\{ \ell n\, \frac{z}{z_{o_c}} - 2\, \ell n \left[\tfrac{1}{2} + \tfrac{1}{2} \left(1 - \frac{9z}{L} \right)^{\frac{1}{2}} \right] \right\} + u_* R_s \right]^{-1} \qquad \frac{z}{L} < 0 \qquad (3\text{-}16)$$

$$v_d = u_* \left[\frac{B}{K} \ell n \frac{z}{z_{o_c}} + \frac{4.7}{K} \frac{z}{L} + u_* R_s \right]^{-1} \qquad \frac{z}{L} > 0$$

(3-16)
continued

Similar equations can also be derived for the wind distribution within the surface layer to permit u_* to be eliminated in favor of the velocity at any desired height.

$$\frac{\bar{u}}{u_*} = \frac{1}{K}\left(\ell n \frac{z}{z_o} - \psi_1 \right) \qquad \frac{z}{L} < 0$$

$$\frac{\bar{u}}{u_*} = \frac{1}{K}\left(\ell n \frac{z}{z_o} + 4.7 \frac{z}{L} \right) \qquad \frac{z}{L} > 0$$

where (3-17)

$$\psi_1 = 2 \ell n\left[\tfrac{1}{2}\left(1 + x_1\right)\right] + \ell n\left[\tfrac{1}{2}\left(1 + x_1^2\right)\right] - 2 \tan^{-1} x_1 + \frac{\pi}{2}$$

with

$$x_1 = \left(1 - 15 \frac{z}{L}\right)^{\frac{1}{4}}$$

For the limiting case of Eq. 3-15 this leads to

$$v_d = \bar{u} \left[\ell n \frac{z}{z_o} \left(B \ell n \frac{z}{z_{o_c}} \right) + R_s \bar{u} \right]^{-1} \qquad (3\text{-}18)$$

From Eq. 3-18 it is evident that the deposition velocity generally increases as the wind velocity and/or the surface roughness increases. However, as the wind velocity continues to increase v_d asymptotically approaches R_s^{-1}. These two generalizations still hold true under non-neutral stability conditions.

LEAF OR OTHER SMOOTH SURFACE LAYER (Region 4)

The degree to which the surface absorbs or chemically reacts with a species is a chemistry/biology problem. It appears that it must be measured empirically. For our sensitivity analysis, we will parameterize it as proportional to the concentration of the species in contact with the surface. The constant of proportionality R_s^{-1} will be considered as a known input. In addition to the surface chemistry problem, there is the aerodynamic problem of transportation of the species through the viscous sublayer next to the surface.

Before considering species diffusion across the sublayer, let us consider momentum transport. In this sublayer, the momentum transport, u_*^2 is given by

$$u_*^2 = \nu \frac{\partial u}{\partial n} \propto \nu \frac{u_\ell}{\delta_s} \tag{3-19}$$

The sublayer thickness δ_s is determined by the minimum size turbulent eddies which can be supported by the turbulent energy which is being dissipated, i.e.,

$$\delta_s \propto \nu/q_s \tag{3-20}$$

The turbulent energy in these smallest eddies is tied to the energy in the large eddies through the cascade process which essentially conserves the energy flowing from one eddy size to the smaller size. Thus,

$$q_s = q_T\left(\frac{\delta_s}{\Lambda}\right)^{1/3} \tag{3-21}$$

and

$$u_*^2 = c_1\left(\frac{\nu}{q_T \Lambda}\right)^{1/4} q_T u_\ell \tag{3-22}$$

From the empirical correlations in Schlichting (21) $c_1 \approx 0.12$.

Equation 3-21 is consistent with an effective eddy diffusivity ($q\Lambda$) which is proportional to $n^{4/3}$. Thus close to the surface Eq. 3-19 may be written as

$$u_*^2 = \left(K_1\, n^{4/3} + \nu\right) \frac{\partial u}{\partial n} \tag{3-23}$$

i.e.,

$$\frac{u}{u_*} = \int_0^n \left(K_1\, n^{4/3} + \nu\right)^{-1} u_*\, dn \tag{3-24}$$

Figure 3-3, which compares Eq. 3-24 with K_1 picked to match at one point with velocity profile data close to the surface, demonstrates that this representation is valid through the transition regime from $u \propto n$ to $u \propto \log n$.

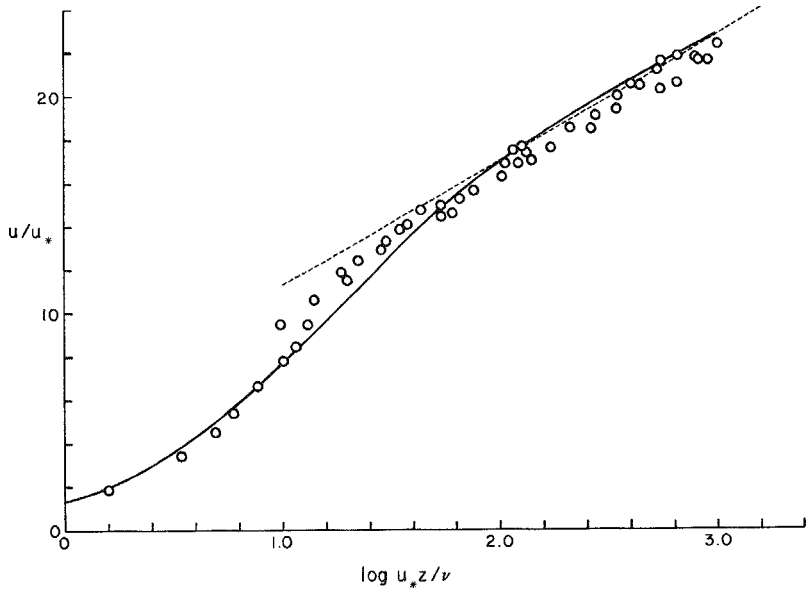

Figure 3-3. Velocity distribution in the sublayer next to a flat surface. Data taken from Reichardt (22).
—— Eq. 3-24. ----- logarithmic variation.

An expression analogous to Eq. 3-24 can be written for either species or heat transfer.

$$\theta - \theta_s = \theta_* u_* \int_0^n \left(\frac{K_1}{B} n^{4/3} + \kappa \right)^{-1} dn \qquad (3\text{-}25)$$

Equations 3-24 and 3-25 can be manipulated to give

$$\theta(\hat{n}) - \theta_s = \theta_* \left(\frac{\nu}{\kappa} \right)^{1/4} (B)^{3/4} \frac{u}{u_*} (n) \qquad (3\text{-}26)$$

with $\hat{n} = \left(\frac{\nu}{\kappa} \right)^{3/4} n$. Since the velocity and temperature (or species) gradients become much smaller outside the sublayer this leads directly to

$$u_* \theta_* = B^{-3/4} (\kappa/\nu)^{1/4} \left(\frac{\nu}{q_T \Lambda} \right)^{1/4} q_T (\theta_\ell - \theta_s) \qquad (3\text{-}27)$$

Equation 3-25 is a valid approximation for κ/ν of order one but is not appropriate for $\kappa/\nu \ll 1$ since the 4/3 exponent is no longer valid for $n \ll \nu/u_*$. Very close to the surface various investigators have approximated ε as proportional to n [Garratt and Hicks (23)], n^2 [Brutsaert (24)], n^3 [e.g., Reichardt (25)], or n^4 [e.g., Deissler (26)]. The currently used model coefficients in our Reynolds stress equation lead to $\varepsilon \sim n^{3.25}$ very close to the surface. These different choices lead to quite different dependences of Eq. 3.27 on κ/ν. The Garratt and Hicks' choice leads to the mass flux proportional to $\ell n(D/\nu)$ while the other dependences of n^2, n^3, $n^{3.25}$ and n^4 lead respectively to the 1/2, 2/3, 0.69 and 3/4-th power of D/ν. Experiments on mass transfer in fluids at high Schmidt numbers ($\nu/D \gg 1$) shown in Figure 3-4 tend to favor the exponent of 2/3. For the case of particle deposition where the Schmidt number based on Brownian motion is quite large we have used 0.7 consistent with our other model coefficients.

When we include in the relation between surface concentration and absorption, the species flux relationship may be written as

$$u_* c_* = \frac{c_1 \left(\frac{D}{\nu} \right)^{0.7} \left(\frac{\nu}{q_T \Lambda} \right)^{1/4} C_\ell q_T}{1 + c_1 \left(\frac{D}{\nu} \right)^{0.7} \left(\frac{\nu}{q_T \Lambda} \right)^{1/4} q_T R_s} \qquad (3\text{-}28)$$

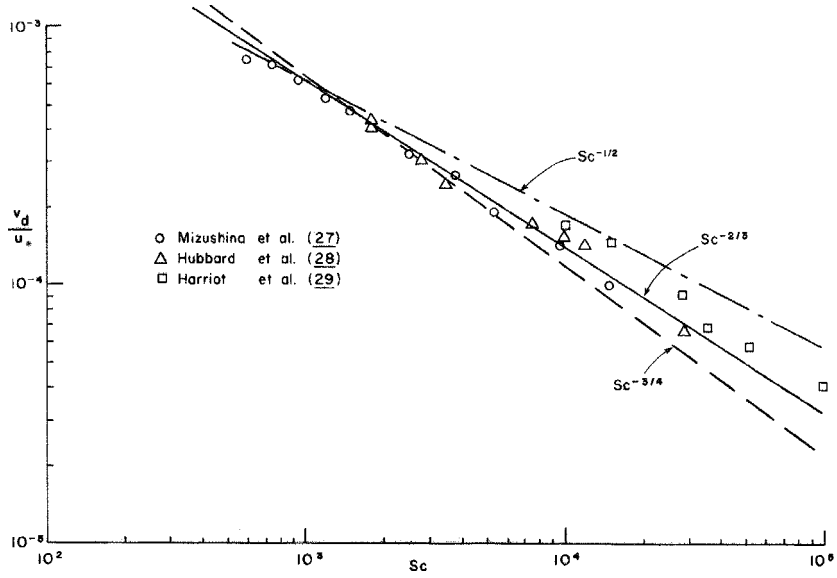

Figure 3-4. Deposition on a flat surface as a function of Schmidt number.

CANOPY FLOW (Region 3)

The lower boundary for atmospheric flows is seldom an aerodynamically smooth, flat surface, so the relations developed in the last section cannot be directly used. The surface is usually covered with some type of vegetal canopy. For flow above the canopy in the constant flux layer, it is possible to characterize the boundary in terms of an effective aerodynamic roughness, z_{oc}; which may or may not be equal to z_o; a top of the canopy deposition velocity v_{d_h}; and a stability parameter L. The purpose here is to see how these parameters are related to the physical characteristics of the canopy.

A second-order closure model for canopy flow has recently been developed by Wilson and Shaw (30). The principal difference between their model and ours is that we consider heat and species transport as well as momentum transport. We also use a somewhat more general representation of the drag per unit volume of the vegetation. Although detailed plant area densities must be given for any type vegetation, the model can predict the variation in species transport as a function of surface Reynolds number, Schmidt number and surface resistance.

The canopy introduces source and sink terms into the basic conservation equations. The skin friction drag forces of the canopy can be estimated by multiplying Eq. 3-22 by total surface area per unit volume. In addition to, and often more important than, the skin friction drag is the pressure drag imposed by the pressure difference between the upwind and downwind surfaces of a leaf or other object in the flow. We will take the profile drag vector as

$$D_{p_i} = c_p\left(\bar{u}_j^2 + q^2\right)^{\frac{1}{2}} A_f \bar{u}_i \tag{3-29}$$

so that the total drag term is given by

$$D_i = \left[c_f A_w + c_p A_f\left(1 + \bar{u}_j^2/q^2\right)^{\frac{1}{2}}\right] q \bar{u}_i \tag{3-30}$$

with

$$c_f = c_1\left(\frac{\nu}{q\Lambda}\right)^{\frac{1}{4}} \tag{3-31}$$

This reduces to the form used by Wilson and Shaw if we set $c_f = q = 0$. There are two reasons for distinguishing between the skin friction drag and the profile drag. First, the species transport to the leaf surface is analogous to only the skin friction portion of the drag. Second, in solving for the turbulent fluctuations within the canopy the energy lost to the mean flow due to profile drag will show up directly as turbulent kinetic energy.

There are two areas appearing in Eq. 3-30; the frontal area per unit volume A_f and the wetted area per unit volume A_w. These two areas differ at least by a factor of two and in a moderate wind when the leaf aligns itself with the wind they can differ by an order of magnitude.

The sink terms in the energy and species equations may be taken from Eqs. 3-26 and 3-27 to be

$$\dot{Q} = c_f\left(\frac{\kappa}{\nu}\right)^{0.7} A_w q\left(\bar{\theta} - \bar{\theta}_s\right) \tag{3-32}$$

$$\dot{C} = c_c A_w q C \tag{3-33}$$

with

$$c_c = c_f \left(\frac{D}{\nu}\right)^{0.7} \Big/ \left[1 + c_f \left(\frac{D}{\nu}\right)^{0.7} q_T R_s\right] \tag{3-34}$$

Both a source and a sink term need to be added to the Reynolds stress equations.

$$\frac{\partial \overline{u_i' u_j'}}{\partial t} = 2c_p \left(\bar{u}_k^2 + q^2\right)^{\frac{1}{2}} A_f \overline{u_i u_j} \, \delta_{ij} - 2c_f A_w q \overline{u_i' u_j'} \qquad \text{(no sum i,j)} \tag{3-35}$$

The first term represents the creation of wake turbulence due to the profile drag while the second recognizes that the skin friction can also dissipate the turbulent fluctuations of velocity. The profile drag can also break up the eddies to increase the dissipation, but this will be accounted for by reducing the dissipation length scale Λ. Following Wilson and Shaw (30), Λ is constrained by

$$\left|\frac{d\Lambda}{dz}\right| \leq 0.65$$

and (3-36)

$$\Lambda \leq \frac{\alpha}{c_p A}$$

with $\Lambda = 0$ at $z = 0$.

The additional terms in the temperature and species correlation equations are modeled as

$$\frac{\partial \overline{\theta' u_i'}}{\partial t} = -c_f A_w q \overline{\theta' u_i'} \left[1 + \left(\frac{\kappa}{\nu}\right)^{0.7}\right] + \ldots \tag{3-37}$$

$$\frac{\partial \overline{c' u_i'}}{\partial t} = -\left(c_f + c_c\right) A_w q \overline{c' u_i'} + \ldots \tag{3-38}$$

$$\frac{\partial \overline{\theta'^2}}{\partial t} = -2c_f \left(\frac{\kappa}{\nu}\right)^{0.7} A_w q \overline{\theta'^2} \tag{3-39}$$

$$\frac{\partial \overline{c'^2}}{\partial t} = -2c_c A_w q \overline{c'^2} + \ldots \tag{3-40}$$

$$\frac{\partial \overline{c'\theta'}}{\partial t} = -A_w q \overline{c'\theta'} \left[\left(\frac{\kappa}{\nu}\right)^{0.7} c_f + c_c\right] \tag{3-41}$$

The complete set of equations and boundary conditions for the transport of momentum, heat, and species within a vegetal canopy are summarized in Appendix A.

With this model it is possible to calculate the function v_{d_h}/u_* needed in Eq. 3-8 as a function of plant characteristics, i.e.,

$$\frac{v_{d_h}}{u_*} = f\left(A_f h,\ h/L,\ R_s u_*,\ A_w/A_f,\ Sc,\ Re\right) \tag{3-42}$$

Shaw et al. (31) measured the flow within a corn canopy with hot-film anemometers. Observations were made at fixed points between rows but variations between similar locations at the same height above the ground were found to be relatively small. In the first set of experiments, measurements include profiles of plant area density (Figure 3-5), mean longitudinal velocities, Reynolds stress, and standard deviations of longitudinal and vertical velocities (Figure 3-6). Wilson and Shaw (30) used $C_p = 0.2$ and $\alpha = 0.1$ to produce best agreement between their computed results and observations.

den Hartog and Shaw (32) reported $C_p = 0.16$ and Uchijima and Wright (33) reported $C_p = 0.17$ when measured scalar wind speed rather than the longitudinal velocity, are used in the drag vector. The plant area density A for a deciduous vegetation is usually measured as the total leaf (upper side only) area per unit volume viewed from the top of the vegetation. The most relevant area in computing the profile drag is the frontal (or cross sectional) area in the direction of the flow, A_f, and hence is generally somewhat less than the traditionally measured plant area. As a result, C_p would be higher than 0.16 if the frontal area A_f is equal to the measured plant area.

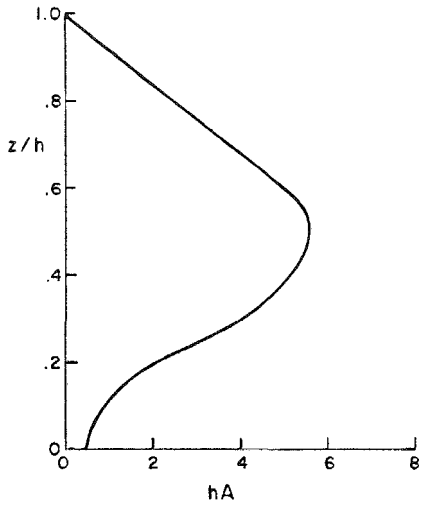

Figure 3-5. Profile of plant area density of corn canopy.

We will use the measured distribution of Ah shown in Figure 3-5 as $A_f h$; $\alpha = 0.1$ and $C_p = 0.16$. This low value of C_p indicates that the frontal area A_f is ≈ 25 percent of the measured leaf area A. $C_1 A_w/A_f$ was given a value of 1 ($C_1 \approx 0.12$, $A_w \approx 8A_f$) such that the skin friction drag is about one-third of the profile drag within the canopy, a relation measured experimentally by Thom (34). Based on these parameters, the equations and boundary conditions as shown in Appendix A are solved and steady-state results are obtained. As shown in Figure 3-6, there is close agreement between computed and observed data. Most of the momentum is absorbed within the upper part of the canopy and little is transported to the ground. The results of our model appear to agree slightly better with observations than those of Wilson and Shaw (30). In particular they appear to have over-estimated σ_u/u_* and σ_w/u_* since skin friction dissipation of turbulent correlations was not accounted for in their model.

The data as shown in Figure 3-7 were taken in October 1971 by Shaw et al. (31). Corn was planted in 76-cm rows; at the start of the experiment the crop was about 290 cm tall and was starting to senesce. By mid-October, few leaves showed any areas of green, the stand was noticeably less dense, and the crop height was reduced to 260 cm. As shown in Figure 3-7, there is good agreement between the computed and observed heat transfer rate within the corn canopy. Various measurements in a corn field (35) have indicated that when u_* increases, the roughness length z_o

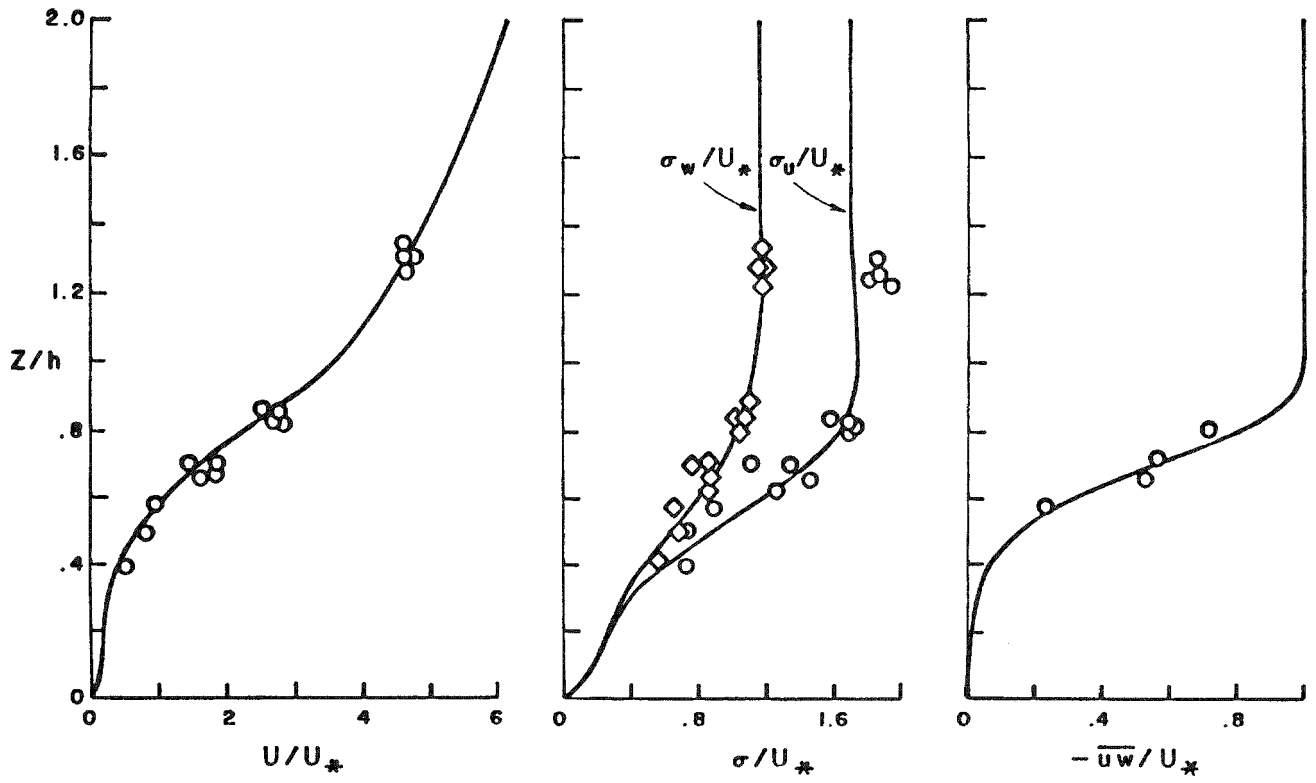

Figure 3-6. Comparison of A.R.A.P. model predictions with data from Shaw et al. (31) in and above a corn canopy.

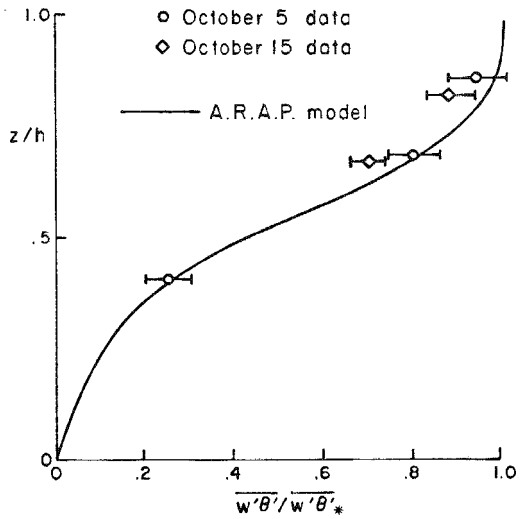

Figure 3-7. Heat transfer within a corn canopy. [Source: Shaw et al. (31)]

increases but zero-plane displacement d decreases. Our model also predicts such trend. When u_* increases from 0.1 m/sec to 1.2 m/sec, z_0/h increases from 0.03 to 0.16, while d/h decreases from 0.9 to 0.5.

Additional calculations in a forest canopy will be presented in later sections to demonstrate the sensitivity of the results to the various parameters indicated in Eq. 3-42.

Section 4

PARTICULATE DEPOSITION

Particles will be diffused by the turbulence in the same manner as a gaseous species as long as the particle is sufficiently small that it can faithfully follow all of the turbulent eddies. This will be true whenever the relaxation time of the particle τ_v, the time required by a particle to reduce its velocity relative to the gas by e^{-1} when acted upon by the fluid drag only, is much less than the eddy time scale Λ/q. Table 4-1 gives some values of τ_v for different size particles with a density of 1 gm/cm^3. Since Λ grows proportional to z near the surface it is possible to estimate the height at which $q\tau_v/\Lambda = 1$ for a given value of q (1 m/sec). At large distances above this height there should be no difference be-

Table 4-1

AEROSOL TRANSPORT PROPERTIES
(Spherical particles with ρ_A = 1 gm/cm^3 in air at 20°C, 1 ATM; and q = 1 m/sec)

Particle diameter 2σ (μm)	Diffusion coefficient D^* (cm^2/sec)	Relaxation time τ_v^* (sec)	Terminal velocity $\tau_v g$ (cm/sec)	Height at which $q \cdot \tau_v/\Lambda = 1$ (m)	Stopping distance / microscale $q^2\tau_v/2\nu$
0.05	2.5×10^{-5}	3.6×10^{-8}	3.5×10^{-5}		1.1×10^{-3}
0.1	6.7×10^{-6}	8.8×10^{-8}	8.6×10^{-5}		2.9×10^{-3}
0.5	6.3×10^{-7}	1.0×10^{-6}	1.0×10^{-3}		3.3×10^{-2}
1.0	2.8×10^{-7}	3.6×10^{-6}	3.5×10^{-3}		0.12
5	4.9×10^{-8}	8.0×10^{-5}	7.8×10^{-2}	12.3×10^{-5}	2.7
10	2.4×10^{-8}	3.2×10^{-4}	3.1×10^{-1}	5×10^{-4}	10.6
50		7.7×10^{-3}	7.58	0.012	2.6×10^{2}
100		3.1×10^{-2}	30.3	0.048	1.0×10^{3}

*Friedlander (36).

tween the turbulent diffusion of a particle and the turbulent diffusion of a gaseous species. For particles with diameters less than a few microns, the table indicates that the only region where the particulate nature of species will generally make any difference is within the surface sublayer. It can also be seen from Table 4-1 that the gravitational settling contribution to deposition velocity of this size particles will generally be quite small.

The particulate nature of the species must be accounted for in estimating the diffusion coefficient within the sublayer. We will account for three contributions to the diffusion of the particle; the Brownian motion of the particle, gravitational settling and inertial impaction. Other mechanisms, such as thermophoresis, diffusiophoretic forces, or electrical migration, which may play a role under certain conditions are discussed in Appendix B. Brownian diffusion is calculable from kinetic theory (36)

$$D_B = \frac{\tilde{c}kT}{3\pi\mu d_p} \tag{4-1}$$

with $\tilde{c}$ a slip correction factor. Some values as a function of particle diameter have been included in Table 4-1.

The mass continuity and momentum equations for a particulate species may be written, following Marble (37), as

$$\frac{\partial c}{\partial t} + \frac{\partial c u_{A_i}}{\partial x_i} = D_B \frac{\partial^2 c}{\partial x_i^2} \tag{4-2}$$

$$\frac{\partial c u_{A_i}}{\partial t} + \frac{\partial c u_{A_i} u_{A_j}}{\partial x_j} = -c \frac{\left(u_{A_i} - u_i\right)}{\tau_v} + c F_i \tag{4-3}$$

where the subscript A on the velocity represents the aerosol velocity, and F_i represents any body force on the particle. Equation 4-2 can be rearranged to read

$$\frac{\partial c}{\partial t} + \frac{\partial c u_i}{\partial x_i} = -\frac{c\left(u_{A_i} - u_i\right)}{\partial x_i} + D_B \frac{\partial^2 c}{\partial x_i^2} \tag{4-4}$$

When the ensemble average concentration and velocities are assumed to be function of only one coordinate normal to a surface, Eq. 4-3 can be used to formally integrate Eq. 4-4 to obtain

$$-v_d C_d = \overline{c'w'} - D_B \frac{\partial C}{\partial n} - \tau_v \left[Cg + \frac{\partial}{\partial n}\left(C\bar{w}_A^2 + C\overline{w_A'^2} + 2\overline{c'w_A'}\,\bar{w}_A + \overline{c'w_A'w_A'} \right) \right] \tag{4-5}$$

The first term on the right hand side is the turbulent transport if the particle follows the fluid velocity which by analogy with Eq. 3-23 is equal to $\frac{4}{3}\varepsilon\, \partial C/\partial n$. The second term is that due to Brownian diffusion. The term in the brackets represents the sum of the contribution from gravitational settling and inertial impaction which we will symbolize as equal to CI. If I is assumed independent of n then Eq. 4-5 may be formally integrated to give

$$v_d = \tau_v I \Bigg/ \left[1 - \exp\left(-\tau_v I \int_0^{z_d} \left(\frac{4\varepsilon}{3} + D_B \right)^{-1} dz \right) \right] \tag{4-6}$$

As seen earlier in Eqs. 3-25 to 3-27

$$\int_0^{z_d} \left(\frac{4\varepsilon}{3} + D_B \right)^{-1} dz = \frac{3}{4} \int_0^{z_d} \left(\varepsilon + \frac{4}{3} D_B \right)^{-1} dz \simeq \left(\frac{3}{4} \right)^{0.3} \left(\frac{D_B}{\nu} \right)^{-0.7} \frac{u(z_d)}{u_*^2}$$

so that Eq. 4-6 may be written as

$$v_d = \tau_v I \Bigg/ \left[1 - \exp\left(-\tau_v I \left(\frac{3}{4} \right)^{0.3} \left(\frac{\nu}{D_B} \right)^{0.7} \frac{u_\ell}{u_*^2} \right) \right] \tag{4-7}$$

We will further approximate Eq. 4-7 as equal to

$$v_d = \tau_v I + \left(\frac{4}{3} \right)^{0.3} \left(\frac{D_B}{\nu} \right)^{0.7} \frac{u_*^2}{u_\ell} \tag{4-8}$$

which never differs from Eq. 4-7 by more than 25 percent.

In an earlier report (38) an attempt was made to derive conservation equations for $\overline{w_A'^2}$ and $\overline{c'w_A'}$ and model the required higher order terms in w_A' to close the system. The result is several new modeling coefficients which must be empirically determined. Rather than pursue this attack in determining I, we will approximate I as equal to

$$\tau_v I = K_2 \frac{q^2 \tau_v}{\delta_s} \left[1 - \exp\left(-K_3 q \tau_v/\delta_s\right)\right] + \tau_v g \qquad (4\text{-}9)$$

The form of Eq. 4-9 is suggested by the bracketted terms in Eq. 4-5. The particle fluctuation velocities in the sublayer can be expected to be proportional to the fluid velocity fluctuations outside the sublayer times a damping factor which is exponentially related to the ratio of the particle stopping distance to the sublayer thickness. For particles bigger than $\approx 10\,\mu m$ diameter it would be necessary to divide Eq. 4-9 by a factor $[1 + K_4(q \tau_v/\Lambda)]^2$ to account for the fact that the particle will not be following the turbulent fluctuations even outside the sublayer. This term will not be included in the current formulation because the largest mass of the sulfate aerosols is believed to consist of particles with diameters around $1\,\mu m$ or less (39).

Friedlander (36) reports that no completely satisfactory theoretical solution to the particle impaction problem exists, but in the regime where deposition is dominated by impaction he develops an expression which has the ratio of the deposition velocity to the shear stress velocity proportional to the square of the ratio of the particle stopping distance to the viscous sublayer thickness. For $q \tau_v/\delta_s \ll 1$, Eq. 4-9 has the same dependence.

When Eq. 3-20 is used for δ_s and empirical information is used to estimate the constants, Eq. 4-9 can be approximated as

$$\tau_v I = 0.1\, c_f q \frac{\tau_v u_*^2}{\nu} \left[1 - \exp\left(-0.08\, q^2 \tau_v/\nu\right)\right] + \tau_v g \qquad (4\text{-}10)$$

This is compared with some data of particles deposited on the underside of a flat plate in the range where inertial deposition dominates (40) in Figure 4-1. In Figure 4-2, the combination of Eq. 4-8 and Eq. 4-10 is compared with Sehmel's (41)

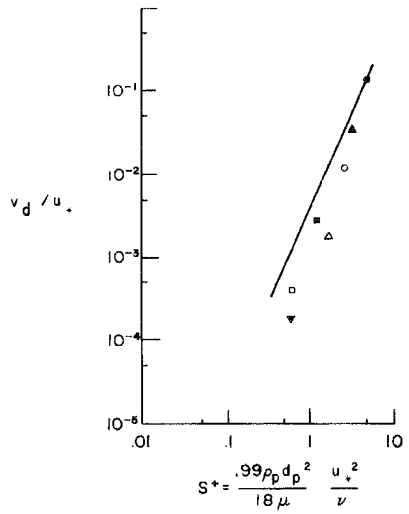

Figure 4-1. Comparison of A.R.A.P. model prediction with Lane & Stukel's deposition data underneath a flat plate (40).

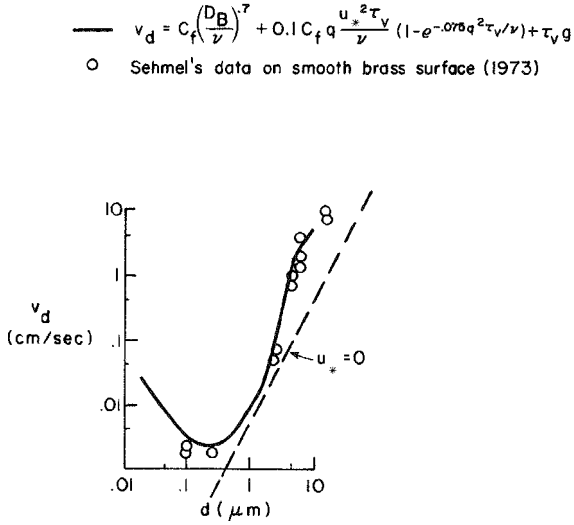

Figure 4-2. Comparison of A.R.A.P. model prediction with Sehmel's deposition data over a smooth brass surface (41). $u_* = 73$ cm/sec, $u_\infty = 1340$ cm/sec.

data for deposition on smooth surface for particles in the transition regime. Both comparisons appear satisfactory. Inclusion of c_f in Eq. 4-10 removes some of the scatter which would be indicated if the data in Figure 4-2 were included on Figure 4-1. Such a summary plot of v_d/u_* versus $\tau_v u_*^2/\nu$ as given by Montgomery and Corn (42) shows considerable scatter.

Considerable uncertainty still surrounds the deposition of particles across the sublayer. As noted in Appendix B, forces neglected in the present analysis can, under certain conditions, dominate deposition over the various range of particle sizes between 0.1 and 1 μm diameter. Also in the real world the particle size distribution is seldom known and may undergo significant shifts due to such things as a sharp gradient in relative humidity and the strong velocity shear in the boundary layer.

For use in our canopy model a factor of 1/3 will be placed in front of the gravitational settling term to approximately account for the fraction of the wetted area which corresponds to the top half of the horizontal projected area.

Section 5

SENSITIVITY ANALYSIS

DEPOSITION WITHIN THE OUTER BOUNDARY LAYER AND CONSTANT FLUX LAYER

Deposition velocity in the outer boundary layer, as shown in Eq. 3-8, is a function of v_{d_h}/u_*, z_o/ℓ, ℓ/L, Ro, z_i/L and distance from the source. We will investigate the sensitivity of $\tilde{v}_{d_\ell}/u_*$ to each of these parameters.

Effect of Canopy Resistance

Figure 5-1 exhibits the dependence of $\tilde{v}_{d_\ell}/u_*$ on v_{d_h}/u_* for three values of ℓ under neutral conditions. As v_{d_h}/u_* increases, the surface resistance decreases until eventually the surface resistance becomes unimportant and hence $\tilde{v}_{d_\ell}/u_*$ is independent of v_{d_h}/u_*. According to Eq. 3-1, the resistance in one region will be important only when it is of the same order as (or larger than) the sum of the other resistances. Consequently, the dependence of deposition velocity on many other parameters can be expected to have similar character as exhibited in Figure 5-1. $\tilde{v}_{d_\ell}/u_*$ as a function of v_{d_h}/u_* during stable conditions (L = 35 m) are shown in Figure 5-2. Due to the increased stability and less mixing of the flow, the dimensionless deposition velocity has an asymptotic value for large v_{d_h} which is less than that for the neutral case by a factor of 5 or more. The differences among the various layer-averaged deposition velocities are also less.

Effect of Surface Roughness Resistance in the Outer Boundary Layer and the Constant Flux Layer

To show the effect of surface roughness $u_*/v_d - u_*/v_{dh} = u_*(R_1 + R_2)$ is plotted against Ro in Figure 5-3. Curve 1 is plotted from Eq. 3-15 and hence indicates u_*R_2. The resistance between the top of the constant flux region and 300 m, as shown by the difference between curve 3 and curve 1, is almost independent of Ro. Curve 2 is under curve 1 since layer-averaged concentration is used in computing the deposition velocity.

Effect of Downwind Distance

Figure 5-4 shows the deposition velocity as a function of downwind distance. The

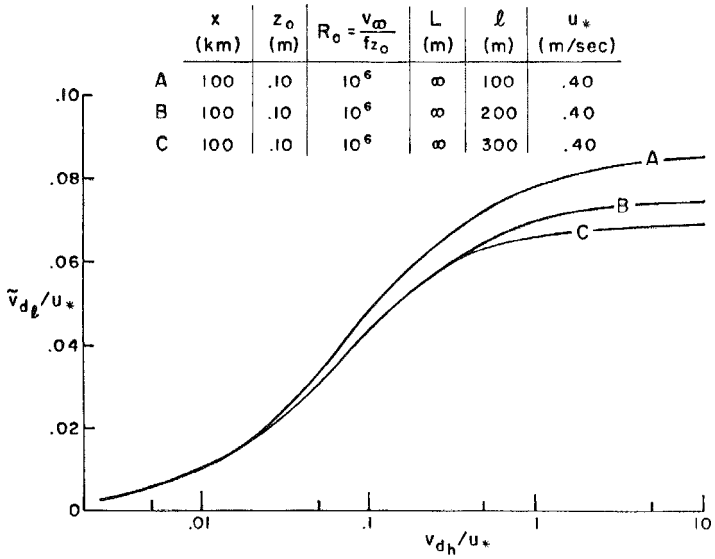

Figure 5-1. Layer averaged deposition velocity for three layer thicknesses as a function of canopy deposition velocity.

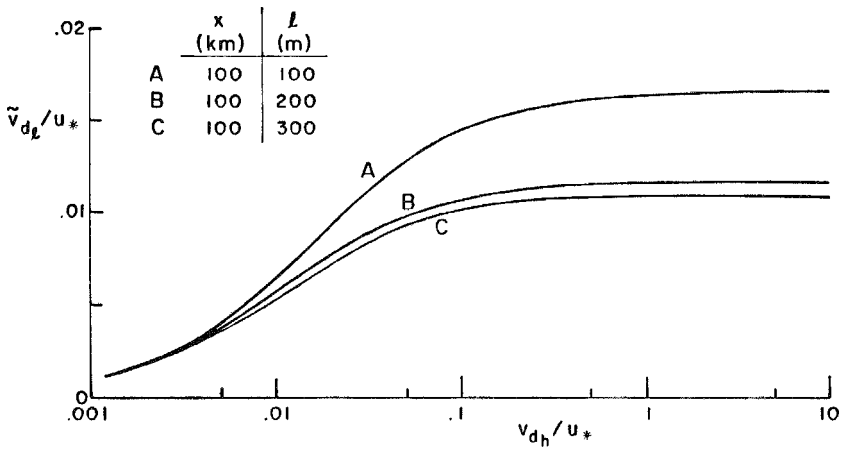

Figure 5-2. Layer averaged deposition velocity for three layer thicknesses under stable conditions as a function of canopy deposition. Ro = 10^6, L = 35 m.

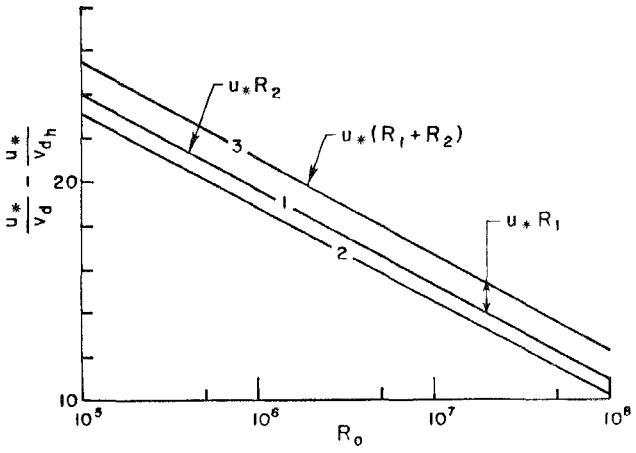

Figure 5-3. Non-surface resistance to deposition as a function of surface roughness given by surface layer function (1) and A.R.A.P. model based on layer averaged deposition velocity (2) and local deposition velocity (3).

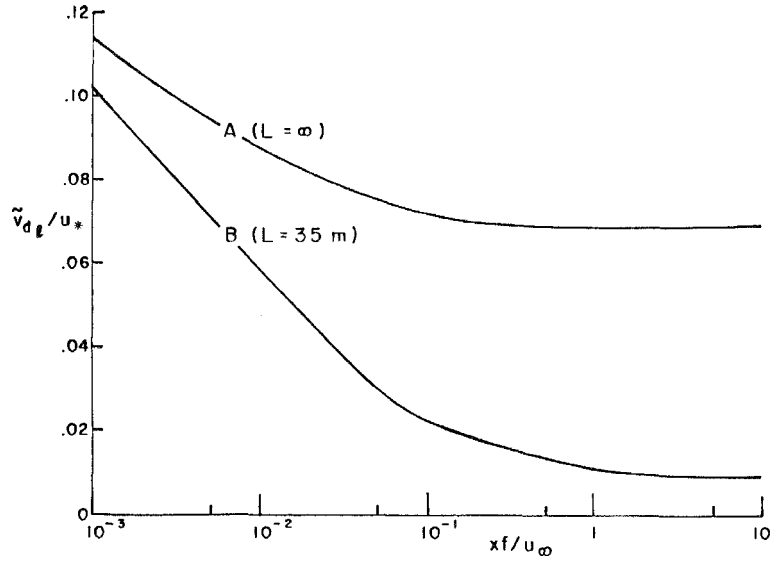

Figure 5-4. Layer-averaged deposition velocity as a function of downwind distance. Ro = 10^6, ℓ = 300 m, v_{d_h}/u_* = 10.

deposition velocity under neutral conditions reaches an asymptotic value after a few kilometers. Under stable conditions, due to the smaller deposition velocity, the initial concentration at higher altitude remains unaffected until relatively longer distance is reached. Consequently, the deposition velocity shows appreciable change even at 10 km. However, the rate of change is much less at farther distances. Also the dependence on distance would be much less if a higher canopy resistance was assumed.

Effect of Stability

The effect of stability on deposition as measured by Eq. 3-16 is shown in Figure 5-5. It shows a strong effect during stable conditions and almost no effect during unstable conditions. Figures 5-6 and 5-7 compare the incremental resistance to deposition computed from the constant flux relations and those computed from the A.R.A.P. boundary layer model. Since the constant flux region only constitutes a small fraction of 300 m in the stable case, large differences can occur (Figure 5-6), but relatively small differences occur in the neutral and unstable cases (Figure 5-7). It is expected that under stable conditions, the simpler equation (3-16) can be employed to accurately estimate the deposition velocities. Under stable conditions, as shown in Figure 5-6, the concentration above 200 m remains unchanged until after 100 km.

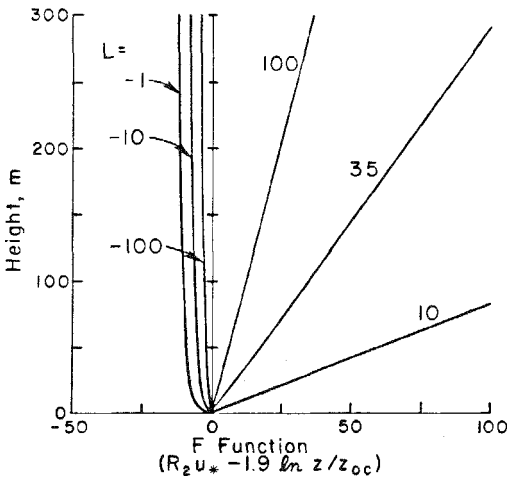

Figure 5-5. Incremental resistance to deposition as a function of height and stability as given by surface layer functions.

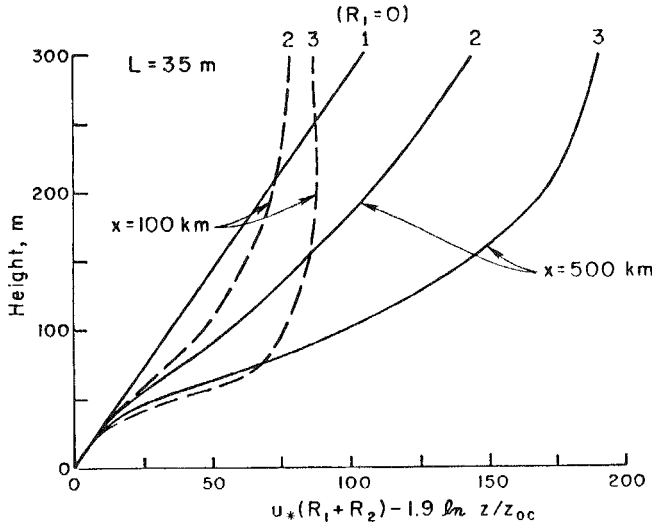

Figure 5-6. Incremental resistance to deposition under stable condition given by surface layer function (1) and A.R.A.P. model based on layer averaged deposition velocity (2) and local deposition velocity (3).

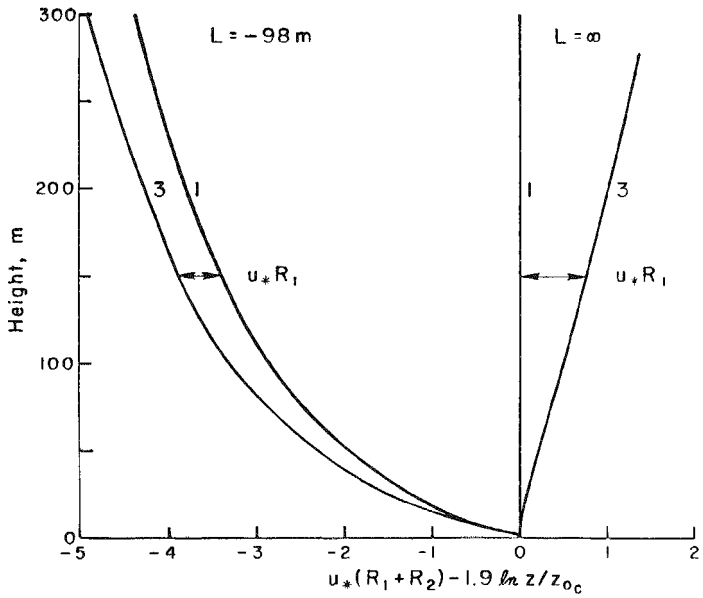

Figure 5-7. Incremental resistance to deposition under neutral and unstable conditions given by surface layer function (1) and A.R.A.P. model based on local deposition velocity (3).

DEPOSITION WITHIN THE CANOPY

The dependence of deposition velocity at the top of a forest canopy (the most common land use of Northeastern U.S.) is also investigated. Figure 5-8 shows the plant structure of the oak forest canopy considered in the present study. The canopy height is taken as 10 m and whenever not specified otherwise A_w/A_f and c_p were assumed to be 8 and 0.16 respectively. Notice that below $z/h \sim 0.4$, the plant area is primarily composed of the tree trunks. The high plant area density near the ground represents the presence of grass and shrub vegetation underneath the forest stand.

The turbulent length scale within the forest canopy satisfying the constraints given by Eq. 3-36 is shown in Figure 5-9. Within the crown height of the canopy, the dense leaves significantly cut down the length scale of the turbulent flow. For the purpose of our sensitivity analysis, the Schmidt number of the gas species is assumed to be 1 (the Schmidt number of SO_2 in air is approximately 0.9).

For a given wind velocity of 5.2 m/sec at twice the canopy height, the wind profile across the canopy is shown in Figure 5-10. Due to the blockage of the dense leaves in the crown height, the effective zero plane is about 74% of the canopy height, while the equivalent roughness length is only about 7% of the canopy height. The

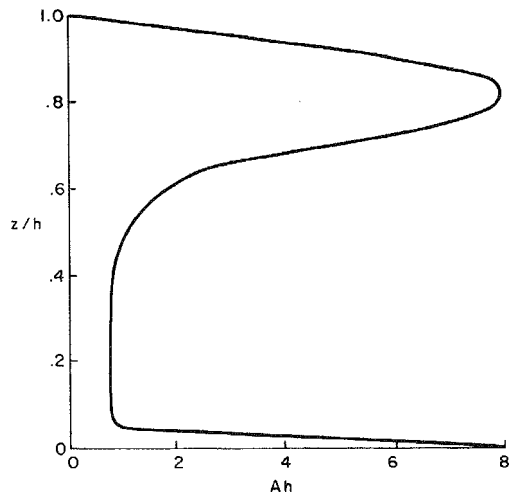

Figure 5-8. Profile of plant area density within a deciduous forest during summer time. Total plant area/unit ground area ≈ 3.

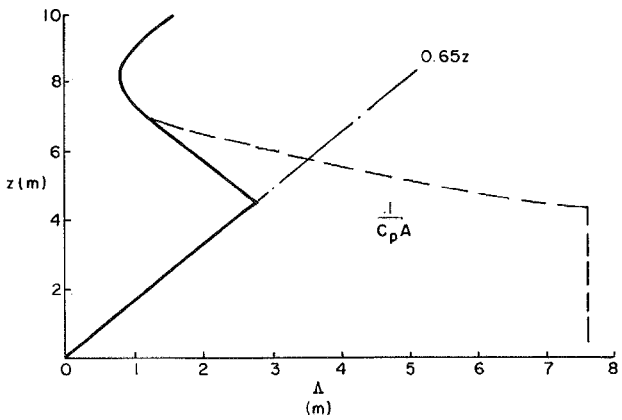

Figure 5-9. Profile of scale length within the summer deciduous forest (solid line) that satisfies the constraints given by Eq. 3-36.

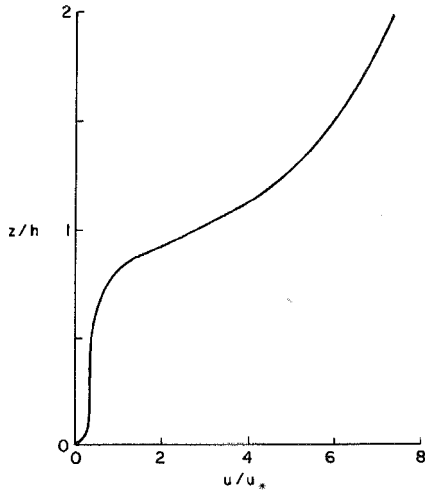

Figure 5-10. Profile of wind velocity within and above the summer deciduous forest. $z_0/h = 0.07$, $d/h = 0.74$, $u_* = 70$ cm/sec.

total profile drag in the canopy for this case is about three times the total friction drag.

One profile as given in Figure 5-10, of course, cannot represent all the wind profiles that may be found in forest canopies under different conditions. That could be the subject of another large report. Cionco (43) has given the wind profiles measured in a variety of different canopies under different conditions. What we are primarily interested in here is the sensitivity of deposition velocities to different conditions. Indications of the sensitivity of deposition velocity in a forest canopy to leaf surface resistance, stability, Schmidt number, leaf shape, wind speed, particle size, and canopy distribution follow.

Effect of Leaf Surface Resistance

Figure 5-11 shows v_{d_h}/u_* as a function of $R_s u_*$, the leaf surface resistance. As $R_s u_*$ decreases, the leaf surface resistance becomes increasingly unimportant and v_{d_h}/u_* approaches an asymptotic value. Figure 5-12 shows z_{0_c}/z_0 as a function of $R_s u_*$ under the same conditions.

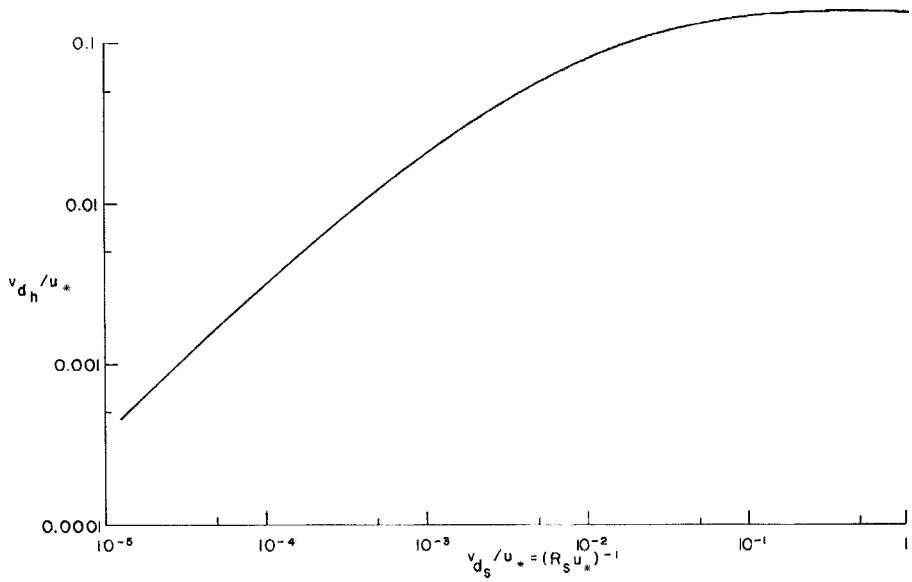

Figure 5-11. Gaseous deposition velocity at the top of the summer deciduous forest as a function of leaf surface resistance. u_{2h} = 5 m/sec, neutral stability.

Effect of Stability

As shown in Figure 5-13, the dimensionless deposition velocity and the friction velocity both decrease as the flow in the forest canopy changes from unstable to neutral and stable conditions. Note that the change in dimensionless v_{dh}/u_* is significantly less than the change in u_*. When h/L increases from - 0.5 to 1.0, u_* decreases from about 1 m/sec to about 0.3 cm/sec.

Effect of Schmidt Number

The deposition velocity increases as D/ν increases, as shown in Figure 5-14. At large D/ν the increase decreases as the sublayer resistance becomes unimportant. Under conditions of higher surface resistance the asymptotic condition would be reached at lower values of D/ν.

Effect of A_w/A_f

As A_w/A_f increases, the effect of skin friction becomes increasingly important. As shown in Figure 5-15, the deposition velocity increases with A_w/A_f and approaches an asymptotic value.

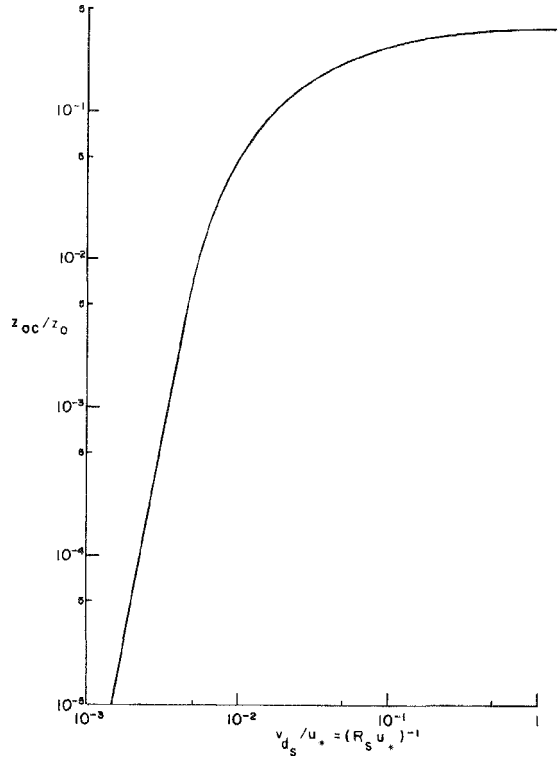

Figure 5-12. Ratio of roughness lengths for gaseous transport in the summer forest. u_{2h} = 5 m/sec, neutral stability.

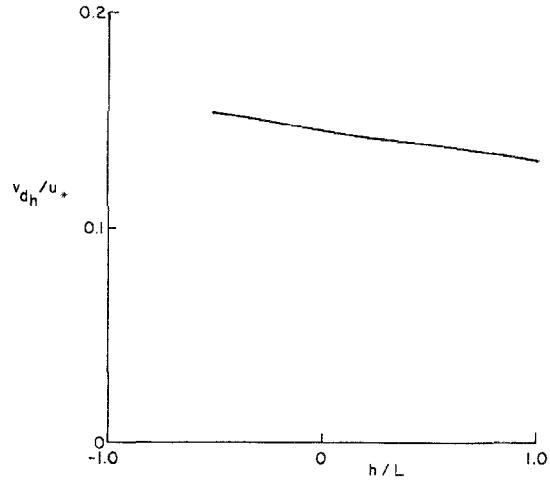

Figure 5-13. Gaseous deposition velocity as a function of stability in the summer forest.

Effect of Wind Speed above the Canopy

As shown in Figure 5-16, the deposition velocity of gas increases with the wind speed at 2h in an almost linear fashion. This is consistent with the sublayer resistance formula developed in previous sections of this report.

Particulate Deposition within the Canopy

Figure 5-17 shows the particulate deposition velocity in a forest canopy as a function of particle size. The minimum deposition velocity which occurs at approximately 0.5 μm particle diameter is increased over that for a flat surface but only by approximately one order of magnitude. The increase is not as much as would appear to be indicated by Sehmel and Hodgson's (14) correlation based on scaling up results from surfaces with much smaller aerodynamic roughness. Two curves are indicated on Figure 5-17 based on using different assumptions regarding the charac-

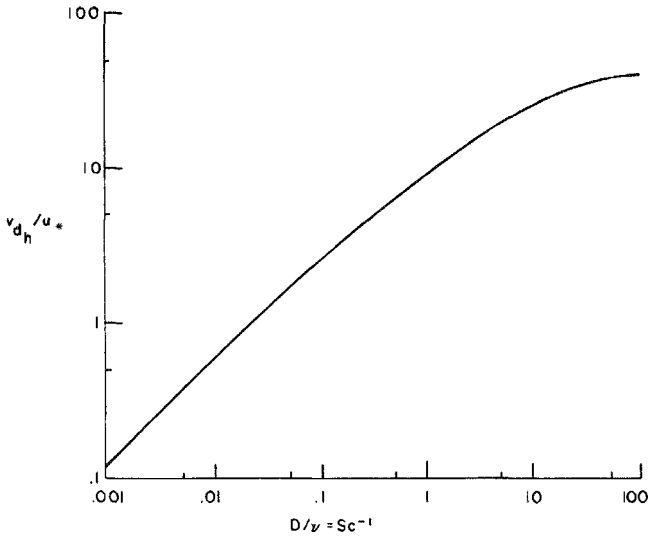

Figure 5-14. Gaseous deposition velocity at the top of the summer forest as a function of Schmidt number. u_{2h} = 5 m/sec, wet foliage, neutral stability.

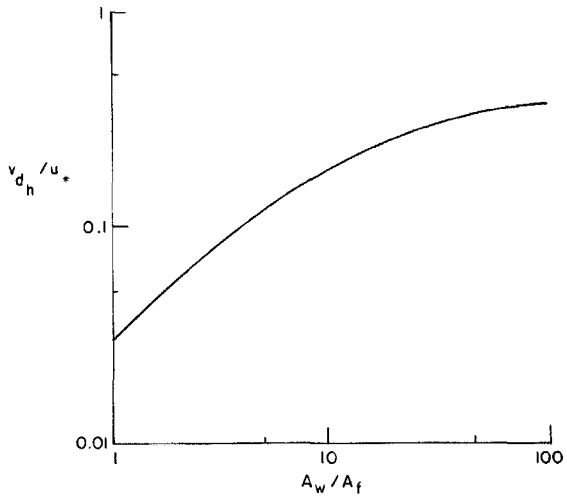

Figure 5-15. Gaseous deposition velocity at the top of the summer forest as a function of A_w/A_f. Plant area index = 3, u_{2h} = 5 m/sec, wet foliage, neutral stability.

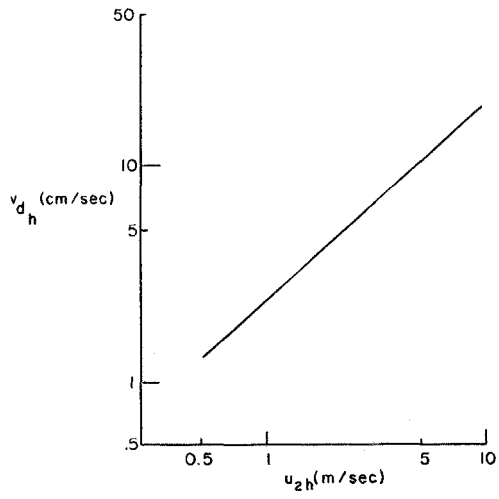

Figure 5-16. Gaseous deposition velocity at the top of the summer forest as a function of u_{2h}. Plant area index = 3, wet foliage, neutral stability.

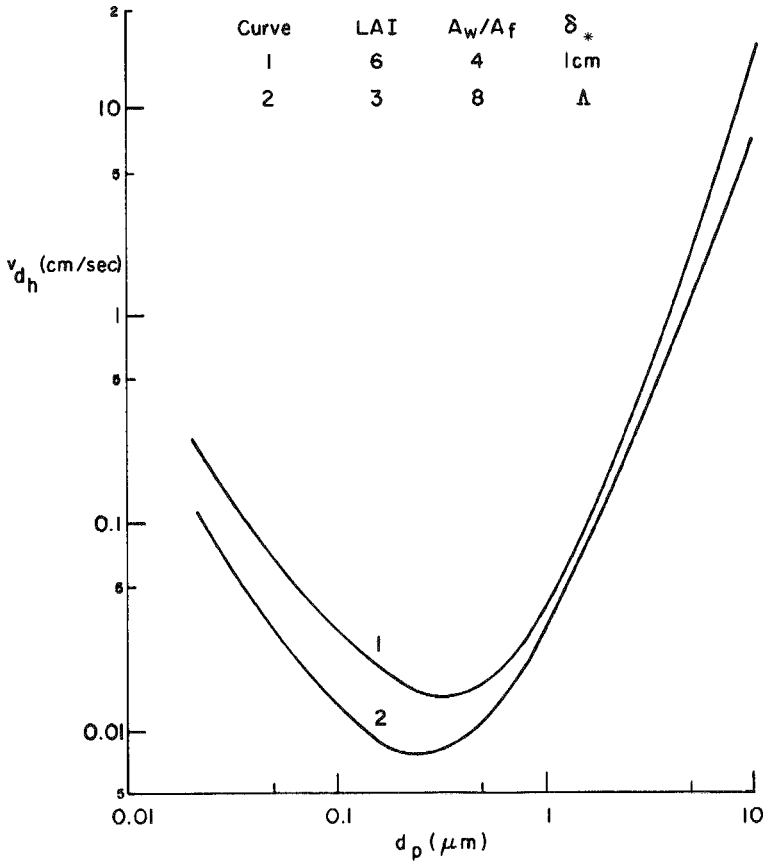

Figure 5-17. Particulate deposition velocity within the summer forest as a function of particle diameter for u_{2h} = 5 m/sec, neutral stability and ρ_p = 1 gm/cm^3.

teristic length and canopy structural characteristics. The resulting differences in deposition velocity represent the uncertainty due to unknowns in the canopy structure.

It should be noted that the result in Figure 5-17 appears to be at odds with the recently reported measurements of Wesely and Hicks (15). They reported deposition velocities as high as 1 cm/sec to a Loblolly pine forest in the afternoon for sulfate particles believed to be in the size range of 0.01 μm to 1 μm diameter. When we attempt to account for differences between the oak and the pine forest we obtain deposition velocities higher than those in Figure 5-17 but still much less than 1 cm/sec. Appendix B speculates on mechanisms ignored from the present analysis which could conceivably be responsible for such a large increase in deposition.

For particles of 0.5 μm diameter, the variation of v_{d_h} as a function of A_w/A_f is shown in Figure 5-18. Variation of v_{d_h}/u_* as a function of u_{2h} is shown in Figure 5-19.

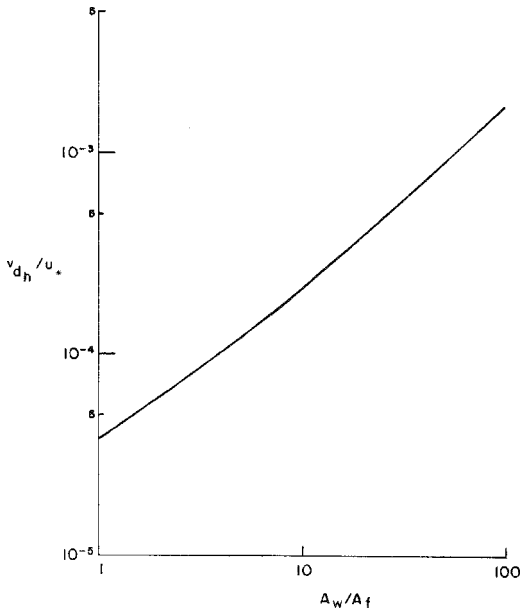

Figure 5-18. Deposition velocity of 0.5 μm-diameter particles at the top of the summer forest as a function of A_w/A_f. u_{2h} = 5 m/sec, neutral stability.

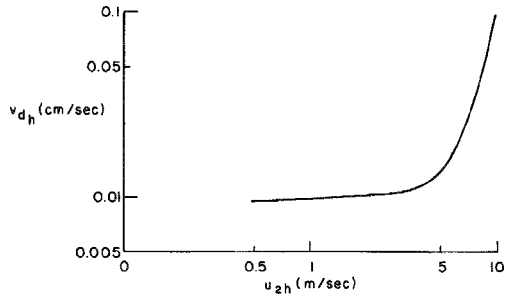

Figure 5-19. Deposition velocity of 0.5 μm-diameter particles at the top of the summer forest as a function of u_{2h}. Neutral stability.

Deposition in Various Canopies

A major portion of the land in the Northeastern United States is covered with deciduous forests. Due to the growth and senescence of the leaves, the plant area density of a deciduous forest varies significantly with season. As shown in Figure 5-20, the plant area density of the forest during winter is only composed of non-leaf area and hence the plant area index (PAI, integral of plant area density) is only a fraction of that during the summer. Some fraction of the land in the Northeastern United States is composed of suburbs with a mixture of houses and isolated trees. It is assumed that the plant area density for a suburban canopy can be represented by a profile such as that shown in Figure 5-20. Based on these profiles, the flow and deposition as affected by the three different types of canopies may

	Plant Area Index
1 Summer Forest	3
2 Winter Forest	1.1
3 Suburb	0.5

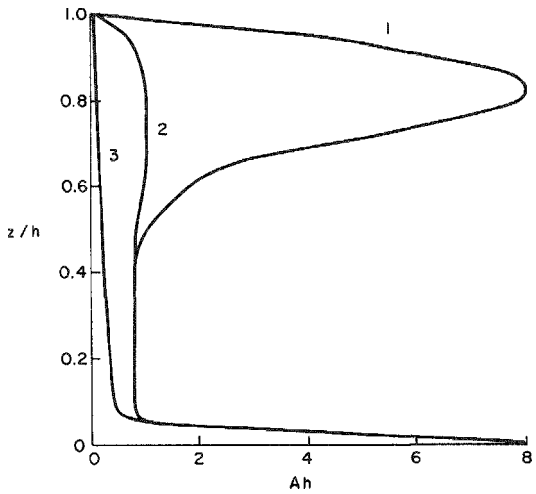

Figure 5-20. Profile of plant area density within a (1) summer forest, (2) winter forest, and (3) suburban canopy with trees and houses.

	z_o/h	d/h
1 Forest (Summer)	.07	.74
2 Forest (Winter)	.26	.013
3 Suburb	.07	0

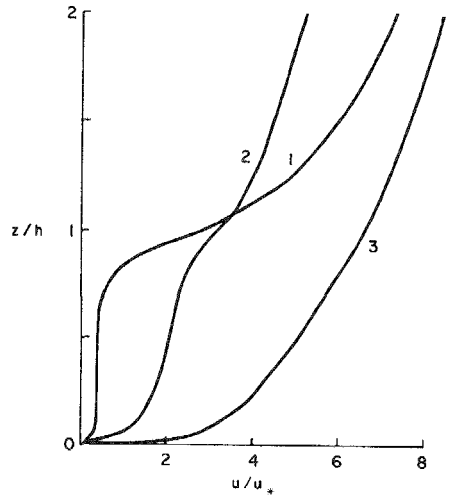

Figure 5-21. Profile of wind velocity within and above (1) summer forest, (2) winter forest, and (3) suburban canopy.

be computed according to our model. The wind distributions are presented in Figure 5-21. In all the calculations, c_p and A_w/A_f were assumed to be 0.16 and 8 respectively. The deposition velocities of gas in the three different kinds of canopies are shown in Figure 5-22. It is interesting to note that the increased penetration of the wind into the winter canopy increases the turbulence sufficiently to counterbalance much of the decrease in v_{d_h}/u_* due to the loss in surface area. Of course, in this comparison, we are assuming essentially no surface resistance, corresponding to a wet canopy.

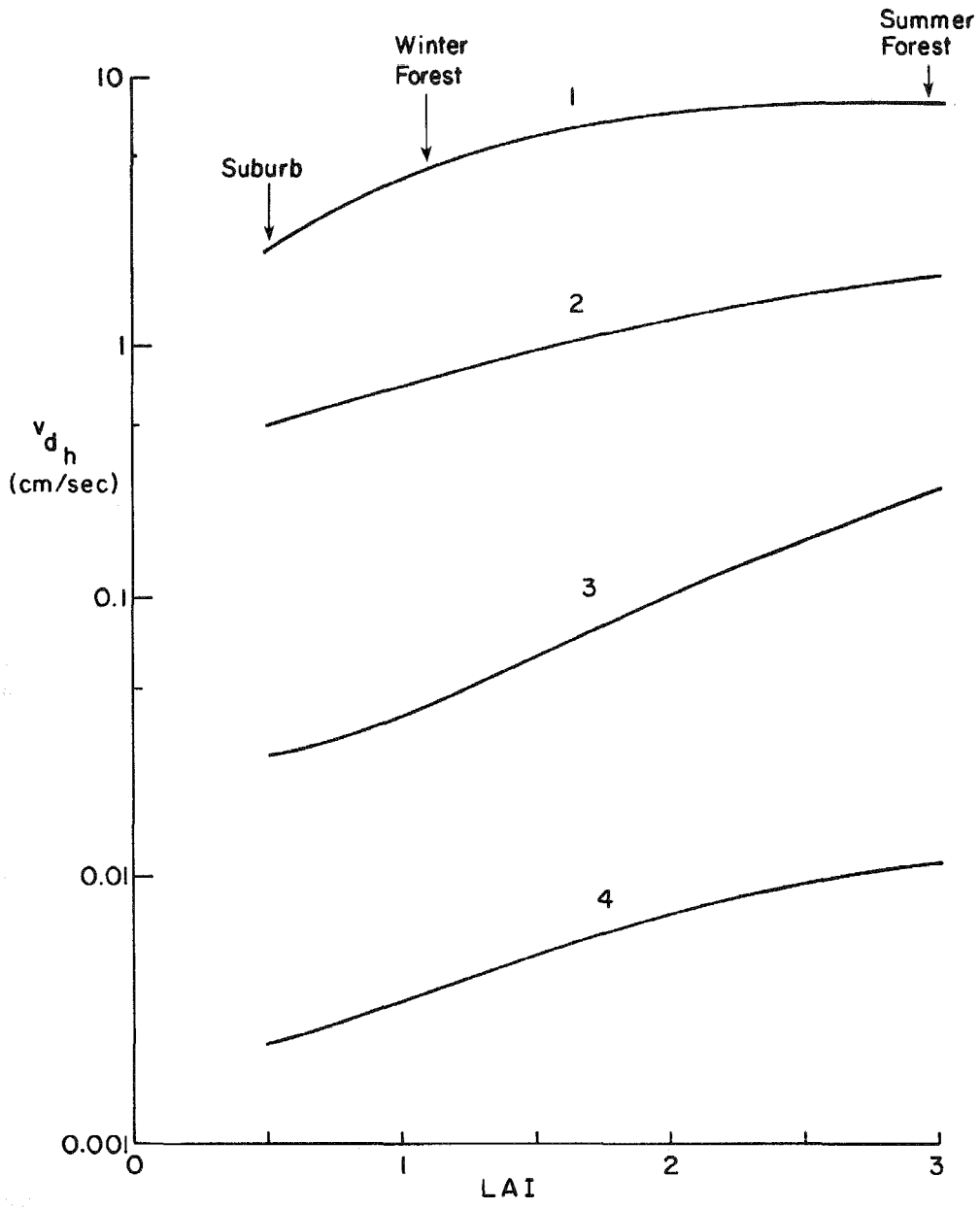

Figure 5-22. Deposition velocity of (1) gas on wet leaves, (2) gas on dry leaves with minimum stomatal resistance, (3) 0.02 μm-diameter particles, and (4) 0.5 μm-diameter particles at the top of the canopy as a function of leaf area index.

Section 6

PARAMETERIZATION FOR REGIONAL MODELS

Dry deposition rates can be an important variable in determining the transport of SO_2 and sulfate aerosols on the regional scale. Our model as developed in the preceding sections is certainly too complicated for use in any practical regional model. Here we will attempt to present a relatively simple parameterization that approximately represents the output of the complete model.

Our procedure will be to start with Eq. 3-1 and parameterize each of the separate resistances. Regional models ordinarily need to deal with a surface drag coefficient in their representation of the wind distribution, so our primary task will be to relate v_d to c_D.

From Eqs. 3-15 and 3-17 it may be deduced that under neutral conditions

$$(R_1 + R_2) = B\left(\frac{\Delta u}{u_*^2}\right) \tag{6-1}$$

This expression does not remain exactly valid over the full range of stability conditions. It yields a value that is slightly high under unstable conditions and low under stable conditions, but it brings in the effect of stability as accurately as it would generally be possible to estimate it over regional areas. Also Eq. 6-1 does not include all the subtleties involved in precisely defining the resistance in the boundary layer above the surface constant flux layer, but as seen in the preceding section these will differ with distance downwind from the source and with the thickness of the bottom layer in the regional model to be considered. However, it is essential to amend Eq. 6-1 to account for the difference between the momentum sinks and the species sinks within the surface canopy.

From the mean species diffusion equation (Eq. A-4)

$$v_{d_h} C_h = \int_0^h c_c A_w q (C - C_s)\, dz \tag{6-2}$$

while from the momentum equation

$$u_*^2 = \int_0^h c_f A_w q\, u\, dz + \int_0^h c_p A_f \left[1 + \frac{u^2}{q^2}\right]^{\frac{1}{2}} q\, u\, dz \tag{6-3}$$

Thus the canopy resistance may be written as

$$R_c u_* = \frac{u_h}{u_*} \left(1 + D_p/D_f\right) \frac{\int_0^h c_f A_w q \left(u/u_h\right) dz}{\int_0^h c_c A_w q \left[\left(C - C_s\right)/C_h\right] dz} \tag{6-4}$$

where D_p/D_f is the ratio of profile drag to skin friction drag. From Eq. 4-8, c_c can be related to c_f

$$c_c = c_f \left(D_B/\nu\right)^{0.7} \left(1 + \frac{R_{Diff}}{R_{Imp}}\right) \tag{6-5}$$

The ratio R_{Diff}/R_{Imp} represents the ratio of the sublayer resistance to diffusion to its resistance to particle inertial impaction. With the aid of Eq. 6-5, Eq. 6-4 may be written as

$$R_c u_h = \frac{\left(1 + D_p/D_f\right) \hat{H}}{C_{D_h} \left(D_B/\nu\right)^{0.7} \left\langle \left(1 + \frac{R_{Diff}}{R_{Imp}}\right) \right\rangle} \tag{6-6}$$

where $\hat{H}$ should be an order one shape parameter

$$\hat{H} = \frac{\int_0^h c_f A_w q \frac{u}{u_h} dz}{\int_0^h c_f A_w q \left[(C - C_s)/C_h\right] dz} \qquad (6\text{-}7)$$

and the angled brackets represent an average throughout the canopy.

Before estimates of $\hat{H}$ can be made it is necessary to examine how distributions of $C - C_s$ typically relate to distributions of u in the canopy. Figure 6-1 shows

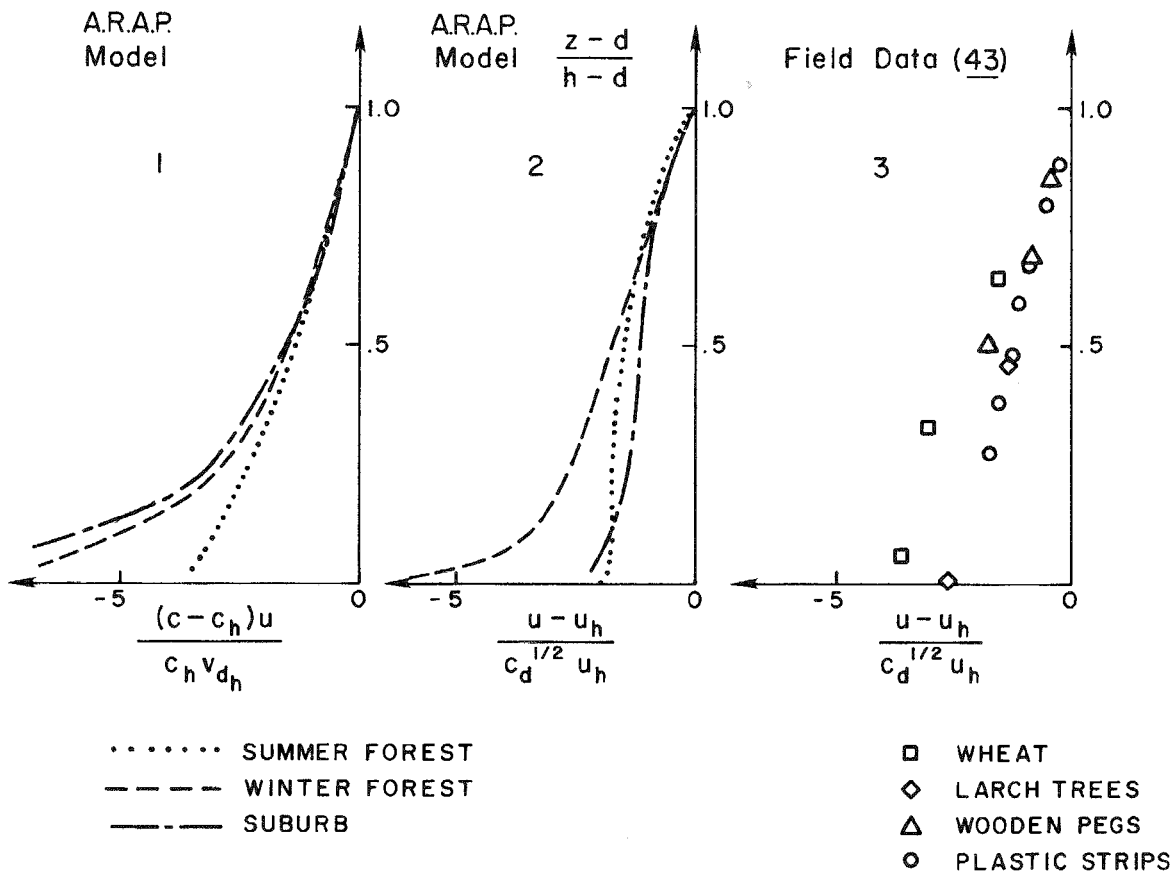

Figure 6-1. Similarity profile of gaseous concentration (1) and wind velocity (2) predicted by A.R.A.P. model and wind velocity measured by various workers (3).

that to a rough approximation

$$\left(\frac{C - C_s}{C_h} - 1\right) R_c u_h = c_{D_h}^{-1}\left(\frac{u}{u_h} - 1\right) \tag{6-8}$$

To the accuracy to which Eq. 6-8 holds it is possible to write 6-7 as

$$\hat{H}^{-1} = H + (1 - H)\left(R_c u_h c_{D_h}\right)^{-1} \tag{6-9}$$

with

$$H = \int_0^h c_f A_w q \, dz \Big/ \int_0^h c_f A_w q \, \frac{u}{u_h} \, dz \tag{6-10}$$

With the aid of Eq. 6-9, Eq. 6-6 can be rearranged to give

$$R_c C_D u_h = H^{-1}\left[\frac{(D/\nu)^{0.7}\left\langle\!\left\langle 1 + R_{Diff}/R_{Imp}\right\rangle\!\right\rangle}{\left(1 + D_p/D_f\right)} - 1\right] + 1 \tag{6-11}$$

When the surface absorption resistance is added to the canopy contribution and the external layer the total resistance may be parameterized as

$$R_t = \frac{3}{4}\frac{\left(u_\ell - u_h\right)}{u_*^2} + \frac{u_h}{u_*^2}\left\{1 + H^{-1}\left[\frac{(\nu/D)^{0.7}\left(1 + D_p/D_f\right)}{\left\langle\!\left\langle 1 + R_{Diff}/R_{Imp}\right\rangle\!\right\rangle} - 1\right]\right\} + \frac{R_s}{LA_w I} \tag{6-12}$$

$$R_t u_\ell = \frac{3}{4} C_D^{-1} + \left(C_D C_{D_h}\right)^{-\frac{1}{2}}\left\{\frac{1}{4} - H^{-1} + H^{-1}\frac{(\nu/D)^{0.7}\left(1 + D_p/D_f\right)}{\left\langle\!\left\langle 1 + R_{Diff}/R_{Imp}\right\rangle\!\right\rangle}\right\} + \frac{R_s u_\ell}{LA_w I} \tag{6-13}$$

Except for approximating the stability variation in the first term on the right hand side of Eq. 6-13 and the approximation involved in Eq. 6-8 this expression still reflects the results of our complete model as long as H, D_p/D_f, C_{D_h} and R_{Diff}/R_{Imp} are taken from the complete model. At this point we make further approximation to the bracketed term in Eq. 6-13 to write it as

$$R_t u_\ell = \frac{3}{4} C_D^{-1} \left[1 + \frac{(\nu/D)^{0.7} (1 + D_p/D_f)}{\langle (1 + LAI)(1 + R_{Diff}/R_{Imp}) \rangle} \right] + \frac{R_s u_\ell}{LA_w I} \qquad (6\text{-}14)$$

(1) (2) (3)

The 3 terms representing (1) resistance to turbulent transport, (2) canopy sublayer resistance, and (3) surface resistance, have different time scales over which they vary. The first term's principal variation is diurnal. Two to three orders of magnitude difference between values at 1 p.m. and 1 a.m. local time is expected. The second term may be expected to only vary seasonally as the canopy structure changes. The last term will vary diurnally as stomata open and close, seasonally as the plant evolves and on a somewhat more random time basis depending upon whether the plant is wet or dry.

Different terms will be important in Eq. 6-13 under different conditions. For example, when considering the deposition of SO_2 to a surface covered with a tall flexible grass covered with dew, the first term on the right hand side of Eq. 6-13 will be the only term making a significant contribution. In this case the last term will be negligible because of the high solubility of SO_2 (unless the pH of the water is low). The remaining terms, after the first term, will be relatively low because the Schmidt number is approximately 1 and the ratio D_p/D_f is small. Under these conditions Reynolds analogy should approximately hold and mass will be diffused to the canopy surfaces in much the same manner as momentum.

Table 6-1 presents some estimates of representative values of the 3 different terms in Eq. 6-13 under different conditions. When indicated, the estimates are obtained from the cited references. The uncited values are either commonly accepted values or our estimate of the particular resistance.

Unfortunately, considerable uncertainty still exists about the last 2 terms in Eq. 6-14. For a gas such as SO_2 the uncertainty in the second term, which represents

Table 6-1

REPRESENTATIVE VALUES OF DEPOSITION RESISTANCE TERMS IN EQ. 6-14
(sec/cm)

	Minimum	Low	Typical	High	Maximum
(1) Aerodynamic turbulent[a]	0.05	0.2	1	5	20
	Unstable flow over rough surface	Modest neutral winds	Light neutral winds	Stable winds	Light stable winds
(2) Laminar sublayer ($R_{S.L.}$)	0.01	0.1	1	20	1000
	Gas species transferred to pine forest	Gas species transferred to smooth surface	0.01 μm particles on pine forest	0.5 μm particles deposited on pine forest under moderate wind conditions	0.5 μm particles deposited on smooth surface
(3) Surface R_s (for SO_2)	0.02	0.2	0.5	1	10
	(Water)	(Calcarious soil)	(Grass or wheat)	(Pine with open stomata)	(Pine with closed stomata)

[a]Total resistance to turbulent transport from the surface sublayer to 100 m height.

the difference between the canopy resistance to momentum transfer and its resistance to mass transfer, will generally not be critical because the other 2 terms will generally be larger. Some improvement in gas deposition estimates may be accomplished by improvements in estimating the surface resistance as a function of the interaction between plant physiology and the atmospheric environment. However, for regional modeling the biggest uncertainties are probably involved in the spatial and time averages required.

The situation is quite different for the deposition of particles. In this case the second term in Eq. 6-14 is both the largest and the most uncertain. Appendix B

discusses several mechanisms which may play a role in determining the size of this term. It is clear that further investigations will be required to significantly reduce the uncertainty in this term.

Section 7

CONCLUDING REMARKS

A model for dry deposition of SO_2 and sulfate aerosol has been presented and a number of calculations made to clarify the role of the critical parameters involved. Based on the results of this detailed model a much simpler parameterized model was also constructed for use with regional models.

Laboratory experiments can play an important role in improving sulfur deposition estimates particularly by investigating the sublayer resistance to fine particulate deposition on natural leaf clusters. However, there remains a need for carefully chosen field experiments to validate parameterization for use in a regional model such as SURE. Such field experiments should be designed to measure SO_2 and sulfate aerosol deposition at a few sites chosen for spatial homogeneity and to represent the different land uses prevalent in the SURE region. At each of these sites data should be taken for a number of different well-documented meteorological and surface conditions. Relatively short time averages (< 1 hr) should be used so that the variation with surface and ambient air environment remain in the data. With such a data set, it should be possible to

(a) use the present or similar model of turbulent diffusion to determine the sum of the surface stomatal and/or absorption resistance and the sublayer viscous resistance;

(b) compare the results at the same site with results for similar conditions but with very small surface resistance (such as wet foliage) to determine the relative contributions of surface and sublayer resistance under different conditions.

This provides the means for estimating separately the 3 contributions to Eq. 6-14.

REFERENCES

1. T. F. Lavery, G. M. Hidy, R. L. Baskett and J. Thracher. "Occurance of Long Range Transport of Sulfur Oxides in the Northeastern United States." In Fourth Symposium on Turbulence, Diffusion and Air Pollution, Preprint Volume, American Meteorological Society, Reno, Nevada, January 1979, pp. 314-321.

2. A. C. Chamberlain. "Dry Deposition of Sulfur Dioxide." Paper presented at the Symposium on Potential Environmental and Health Effects of Atmospheric Sulfur Deposition, Oak Ridge National Laboratory, Oak Ridge, Tennessee, October 1979.

3. T. A. McMahon and P. J. Denison. "Empirical Atmospheric Deposition Parameters - A Survey." Atmospheric Environment, Vol. 13, 1979, pp. 571-585.

4. R. B. Husar, J. P. Lodge, Jr., and D. J. Moore (Editors). Sulfur in the Atmosphere, Proceedings of the International Symposium, Dubrovnik, Yugoslavia, September 1978, 816 pp.

5. J. A. Garland. "Dry and Wet Removal of Sulfur from the Atmosphere." Atmospheric Environment, Vol. 12, 1978, pp. 349-362.

6. E. B. Fowler. "Dry Deposition of SO_2 on Agricultural Crops." Atmospheric Environment, Vol. 12, 1978, pp. 369-373.

7. P. S. Liss and P. G. Slatter. "Mechanism and Rate of Gas Transfer Across the Air-Sea Interface. Atmosphere-Surface Exchange of Particulate and Gaseous Pollutants." ERDA Symposium, Series 38, 1976, pp. 354-368.

8. M. L. Weseley and B. B. Hicks. "Some Factors that Affect the Deposition Rates of Sulfur Dioxide and Similar Gases on Vegetation." APCA Journal, Vol. 27, 1977, pp. 1110-1116.

9. G. A. Sehmel and S. L. Sutter. "Particle Deposition Rates on a Water Surface as a Function of Particle Diameter and Air Velocity." J. de Rech. Atmos., Vol. 8, 1974, pp. 911-920.

10. J. G. Droppo. "Summary of Field Data on Dry Removal Rates of Gases and Particles from the Atmosphere." Pacific Northwest Laboratory Annual Report, Part 3 - Atmospheric Sciences (J. Hales, editor), BNWL-2100, Pacific Northwest Laboratory, Richland, Washington, 1976.

11. S. E. Lindberg, R. C. Harriss, R. R. Turner, D. S. Schriner, and D. D. Huff. "Mechanisms and Rates of Atmospheric Deposition of Selected Trace Elements and Sulfate to a Deciduous Forest Watershed." ORNL/TM-6674, Oak Ridge National Laboratory, Oak Ridge, Tennessee, 514 pp.

12. C. M. Sheih, M. L. Weseley and B. B. Hicks. "Estimated Dry Deposition Velocities of Sulfur Over the Eastern United States and Surrounding Regions." Atmospheric Environment, Vol. 13, 1979, pp. 1361-1368.

13. W. G. N. Slinn. "Dry Deposition and Resuspension of Aerosol Particles - A New Look at Some Old Problems. Atmospheric Surface Exchange of Particulate and Gaseous Pollutants." ERDA Symposium, Series 38, 1976, pp. 1-40.

14. G. A. Sehmel and W. H. Hodgson. "Predicted Dry Deposition Velocities. Atmospheric-Surface Exchange of Particulate and Gaseous Pollutants." Energy Research and Development Administration Symposium, Series 38, 1976, pp. 399-422.

15. M. L. Weseley and B. B. Hicks. "Dry Deposition and Emission of Small Particles at the Surface of the Earth." Fourth Symposium on Turbulence, Diffusion, and Air Pollution, Preprint Volume, American Meteorological Society, Reno, Nevada, January 1979.

16. C. duP. Donaldson. "Atmospheric Turbulence and the Dispersal of Atmospheric Pollutants." Workshop on Micrometeorology (D. A. Haugen, editor) Science Press, 1973, pp. 313-390.

17. W. S. Lewellen and M. E. Teske. "Second-Order Closure Modeling of Diffusion in the Atmospheric Boundary Layer." Boundary Layer Meteorology, Vol. 10, 1976, pp. 69-90.

18. J. A. Businger, J. C. Wyngaard, Y. Izumi and E. F. Bradley. "Flux Profile Relationships in the Atmospheric Surface Layer." Journal of Atmospheric Sciences, Vol. 28, 1971, pp. 181-189.

19. W. S. Lewellen and M. E. Teske. "Prediction of the Monin-Obukhov Similarity Functions from an Invariant Model of Turbulence." Journal of Atmospheric Sciences, Vol. 30, 1973, pp. 1340-1345.

20. R. A. Brown. Analytical Methods in Planetary Boundary-Layer Modeling. Halsted Press, 1974, 148 pp.

21. H. Schlichting. Boundary-Layer Theory. Sixth Edition. McGraw-Hill Book Co., 1968, 747 pp.

22. H. Reichardt. "Die Warmeubertragung in Turbulenten Reibungsschichten." Z. Angew. Math Mech., Vol. 20, 1940, pp. 297-328.

23. J. R. Garrett and B. B. Hicks. "Momentum, Heat and Water Vapor Transfer to and from Natural and Artificial Surfaces." Quart. J. R. Met. Soc., Vol. 99, 1973, pp. 680-687.

24. W. Brutsaert. "The Roughness Length for Water Vapor, Sensible Heat and Other Scales." Journal of Atmospheric Sciences, Vol. 32, 1975, p. 2028.

25. H. Reichardt. "The Principles of Turbulent Heat Transfer." Archiv. Ges. Warmetech., Vol. 617, 1951, pp. 129-142.

26. R. G. Deissler. "Convective Heat Transfer and Friction in Flow of Liquids." Turbulent Flows and Heat Transfer (C. C. Lin, editor), Princeton University Press, 1959, pp. 288-338.

27. T. Mizushina, F. Ogino, Y. Oka and H. Fukuda. "Turbulent Heat and Mass Transfer between Wall and Fluid Streams of Large Prandtl and Schmidt Numbers." International Journal of Heat and Mass Transfer, Vol. 14, 1971, pp. 1705-1716.

28. D. W. Hubbard and E. N. Lightfoot. "Correlation of Heat and Mass Transfer Data for High Schmidt and Reynolds Numbers." I/EC Fundamentals, Vol. 5, 1966, p. 370.

29. P. Harriott and R. M. Hamilton. "Solid-Liquid Mass Transfer in Turbulent Pipe Flow." Chem. Engng. Sci., Vol. 20, 1965, p. 1073.

30. N. R. Wilson and R. H. Shaw. "A Higher-Order Closure Model for Canopy Flow." Journal of Applied Meteorology, Vol. 16, 1977, pp. 1197-1205.

31. R. H. Shaw, R. H. Silversides and G. W. Thurtell. "Some Observations of Turbulence and Turbulent Transport Within and Above Plant Canopies." Boundary-Layer Meteorology, Vol. 5, 1974, pp. 429-449.

32. G. den Hartog and R. H. Shaw. "A Field Study of Atmospheric Exchange Processes with a Vegetative Canopy." Heat and Mass Transfer in the Biosphere, 1975, pp. 299-309.

33. Z. Uchijima and J. L. Wright. "An Experimental Study of Air Flow in a Corn Plant-Air Layer." Bull. Nat. Inst. Agric. Sci. Japan, Vol. A11, 1964, pp. 19-65.

34. A. S. Thom. "Momentum, Mass and Heat Exchange of Plant Communities." Vegetation and the Atmosphere, Vol. 2, 1975, pp. 57-109.

35. Z. Uchijima. "Maize and Rice." Vegetation and the Atmosphere, Vol. 1, 1975, pp. 33-64.

36. S. K. Friedlander. Smoke, Dust and Haze. John Wiley and Sons, 1977, 312 pp.

37. F. E. Marble. "Dynamics of Dusty Gases." Annual Review of Fluid Mechanics, Vol. 2, 1970, pp. 397-446.

38. W. S. Lewellen, D. A. Oliver, M. E. Teske, H. Segur and O. Cote. Status Report on "Low-Level, Atmospheric Turbulence Model for Marine Environments." A.R.A.P. Report No. 320, Nov. 1977.

39. K. T. Whitby. "The Physical Characteristics of Sulfur Aerosols." Atmospheric Environment, Vol. 12, 1978, pp. 135-159.

40. D. D. Lane and J. J. Stukel. "Aerosol Deposition on a Flat Plate." Journal of Aerosol Science, Vol. 9, 1978, pp. 191-197.

41. G. A. Sehmel. "Particle Eddy Diffusivities and Deposition Velocities for Isothermal Flow and Smooth Surfaces." Aerosol Science, Vol. 4, 1973, pp. 125-138.

42. T. L. Montgomery and M. Corn. "Aerosol Deposition in a Pipe with Turbulent Airflow." Journal of Aerosol Science, Vol. 1, 1970, pp. 185-213.

43. R. M. Cionco. "Application of the Ideal Canopy Flow Concept to Natural and Artificial Roughness Elements." R & D Report ECOM-5372, U. S. Army Electronics Command, 1971, 63 pp.

44. J. W. Fitzgerald. "Approximation Formulas for the Equilibrium Size of an Aerosol Particle as a Function of Its Dry Size and Composition and the Ambient Relative Humidity." Journal of Applied Meteorology, Vol. 14, 1975, pp. 1044-1049.

45. P. J. Whitmore and A. Meisen. "Diffusiophoretic Particle Collection Under Turbulent Conditions." Atmospheric Environment, Vol. 9, 1978, pp. 135-145.

46. P. G. Jarvis, G. B. James and J. J. Landsberg. "Coniferous Forest." Vegetation and the Atmosphere (J. L. Montieth, editor) Academic Press, 1975, pp. 171-241.

Appendix A

SUMMARY OF EQUATIONS AND BOUNDARY CONDITIONS FOR DIFFUSION IN A CANOPY

In the present study, although we are primarily interested in the steady-state solution, the one-dimensional nonsteady equations are solved. The mean flow equations are:

$$\frac{\partial \bar{u}_i}{\partial x_i} = 0 \tag{A-1}$$

Momentum

$$\frac{D\bar{u}_i}{Dt} = -\left[c_f A_w + c_p A_f \left(1 + \bar{u}_j^2/q^2\right)^{\frac{1}{2}}\right] q\bar{u}_i - \frac{\partial \overline{u_i' u_j'}}{\partial x_j} + \frac{\partial}{\partial x_j}\left(\nu \frac{\partial \bar{u}_i}{\partial x_j}\right)$$

$$- \frac{1}{\rho}\frac{\partial p}{\partial x_i} + \frac{g_i \bar{\theta}}{T_o} - 2\varepsilon_{ijk}\,\Omega_j \bar{u}_k \tag{A-2}$$

Diffusion of heat

$$\frac{D\bar{\theta}}{Dt} = - c_f(\kappa/\nu)^{0.7} A_w q(\bar{\theta} - \bar{\theta}_s) - \frac{\partial \overline{u_i' \theta'}}{\partial x_i} + \frac{\partial}{\partial x_i}\left(\kappa \frac{\partial \theta}{\partial x_i}\right) \tag{A-3}$$

Diffusion of species

$$\frac{DC}{Dt} = - c_c A_w q C - \frac{\partial\left(\overline{u_i' c} - \tau_v g C\right)}{\partial x_i} + \frac{\partial}{\partial x_i}\left(D \frac{\partial C}{\partial x_i}\right) \tag{A-4}$$

In addition, there are six equations for Reynolds stresses:

$$\frac{D\overline{u_i'u_j'}}{Dt} = 2c_p\left(\bar{u}_k^2 + q^2\right)^{\frac{1}{2}} A_f \bar{u}_i \bar{u}_j \, \delta_{ij(\text{no sum } i,j)} - 2c_f A_w q \overline{u_i'u_j'} - \overline{u_i'u_k'} \frac{\partial \bar{u}_j}{\partial x_k}$$

$$- \overline{u_j'u_k'} \frac{\partial \bar{u}_i}{\partial x_k} + \frac{g_i \overline{u_j'\theta'}}{T_o} + \frac{g_j \overline{u_i'\theta'}}{T_o} - 2\varepsilon_{ik\ell} \Omega_k \overline{u_\ell'u_j'} - 2\varepsilon_{j\ell k} \Omega_\ell \overline{u_k'u_k'}$$

$$+ 0.3 \frac{\partial}{\partial x_k}\left(q\Lambda \frac{\partial \overline{u_i'u_j'}}{\partial x_k}\right) - \frac{q}{\Lambda}\left(\overline{u_i'u_j'} - \delta_{ij} \frac{q^2}{3}\right) - \delta_{ij} \frac{q^3}{12\Lambda} \qquad \text{(A-5)}$$

three equations for the heat fluxes

$$\frac{D\overline{u_i'\theta'}}{Dt} = - c_f A_w q \overline{u_i'\theta'} \left[1 + (\kappa/\nu)^{0.7}\right] - \overline{u_i'u_j'} \frac{\partial \bar{\theta}}{\partial x_j} - \overline{u_j'\theta'} \frac{\partial u_i}{\partial x_j} + \frac{g_i \overline{\theta'^2}}{T_o}$$

$$- 2\varepsilon_{ijk} \Omega_j \overline{u_k'\theta'} + 0.3 \frac{\partial}{\partial x_j}\left(q\Lambda \frac{\partial \overline{u_i'\theta'}}{\partial x_j}\right) - \frac{0.75q}{\Lambda} \overline{u_i'\theta'} \qquad \text{(A-6)}$$

three equations for the species fluxes:

$$\frac{D\overline{u_i'c'}}{Dt} = - (c_f + c_c) A_w q \overline{u_i'c'} - \overline{u_i'u_j'} \frac{\partial C}{\partial x_j} - \overline{u_j'c'} \frac{\partial \bar{u}_i}{\partial x_j} + \frac{g_i \overline{\theta'c'}}{T_o}$$

$$- 2\varepsilon_{ijk} \Omega_j \overline{u_k'c'} + 0.3 \frac{\partial}{\partial x_j}\left(q\Lambda \frac{\partial \overline{u'c'}}{\partial x_j}\right) - \frac{0.75q}{\Lambda} \overline{u_i'c'} \qquad \text{(A-7)}$$

and three equations for the scalar correlations of temperature and species

$$\frac{D\overline{\theta'^2}}{Dt} = - 2c_f(\kappa/\nu)^{0.7} A_w q \overline{\theta'^2} - 2\overline{u_j'\theta'} \frac{\partial \bar{\theta}}{\partial x_j} + 0.3 \frac{\partial}{\partial x_j}\left(q\Lambda \frac{\partial \overline{\theta'^2}}{\partial x_j}\right) - \frac{0.45q}{\Lambda} \overline{\theta'^2}$$

(A-8)

$$\frac{D\overline{c'^2}}{Dt} = -2c_c A_w q \overline{c'^2} - 2\overline{u_j c'} \frac{\partial C}{\partial x_j} + 0.3 \frac{\partial}{\partial x_j}\left(q\Lambda \frac{\partial \overline{c'^2}}{\partial x_j}\right) - \frac{0.45q}{\Lambda} \overline{c'^2} \tag{A-9}$$

$$\frac{D\overline{c'\theta'}}{Dt} = -\left[c_c + (\kappa/\nu)^{0.7} c_f\right] A_w q \overline{c'\theta'} - \overline{u_j' c'} \frac{\partial \bar{\theta}}{\partial x_j} - \overline{u_j' \theta'} \frac{\partial C}{\partial x_j}$$

$$+ 0.3 \frac{\partial}{\partial x_j}\left(q\Lambda \frac{\partial \overline{c'\theta'}}{\partial x_j}\right) - \frac{0.45q}{\Lambda} \overline{c'\theta'} \tag{A-10}$$

The above equations reduce to those describing the flow outside the canopy when $c_p = c_f = c_c = 0$. The scale equation is as shown in Eq. 3-36. To study the flow and diffusion within a canopy, the top boundary of the domain of calculation is usually taken at twice the canopy height. At $z = 2h$, the boundary conditions are:

$$\bar{u} = \tilde{u}$$

$$\bar{v} = \tilde{v} = 0$$

$$\bar{w} = 0$$

$$\bar{\theta} = \text{constant}$$

$$C = \text{constant}$$

$$\frac{\partial \overline{u'w'}}{\partial z} = \frac{1}{\rho}\frac{\partial p}{\partial x} = 0 \tag{A-11}$$

$$\frac{\partial \overline{v'w'}}{\partial z} = -\frac{1}{\rho}\frac{\partial p}{\partial y} = 0$$

$$\frac{\partial \overline{u'v'}}{\partial z} = \frac{\partial \overline{u'u'}}{\partial z} = \frac{\partial \overline{v'v'}}{\partial z} = \frac{\partial \overline{w'w'}}{\partial z} = 0$$

$$\frac{\partial \overline{u_i'\theta'}}{\partial z} = \frac{\partial \overline{u_i'c'}}{\partial z} = \frac{\partial \overline{\theta'^2}}{\partial z} = \frac{\partial \overline{c'^2}}{\partial z} = \frac{\partial \overline{c'\theta'}}{\partial z} = 0$$

The lower boundary extends all the way to $z = 0$, at which:

$$\bar{u} = \bar{v} = \bar{w} = 0$$

$$\theta = \text{constant}$$

$$C = -\overline{w'c'}R$$

$$\overline{w'\theta'} = C_1(K/\nu)^{0.7}\,(\nu/q\Lambda)^{1/4}\,q(\bar{\theta}_+ - \bar{\theta}) \qquad \text{(A-12)}$$

$$\overline{w'c'} = C_1(D/\nu)^{0.7}\,(\nu/q\Lambda)^{1/4}\,q(C_+ - C)$$

$$\frac{\partial}{\partial z}(\text{all other turbulent fluxes}) = 0$$

where R indicates the ground resistance to deposition and $+$ represents the value just above the surface. When R is given, expressions for C and $\overline{w'c'}$ may be combined to give a relation between $\overline{w'c'}$ and C_+. The value of C_+ and θ_+ at the bottom grid point are determined by solving the averaged conservation equations for the half-cell adjacent to the ground. Averaged values of Λ and D over the half grid cell are generally used in the expressions for $\overline{w'\theta'}$ and $\overline{w'c'}$. When initial conditions on all the variables are given, the complete solution can then be obtained.

By proper nondimensionalization of the above system of equations and boundary conditions, one can show that the dimensionless deposition velocity at the top of canopy, v_{d_h}/u_*, is a function of A_f, h/L, v_{d_s}/u_*, A_w/A_f, Sc and canopy Reynolds number $\tilde{u}h/\nu$.

From the steady-state flow profiles above the canopy, one can determine an equivalent roughness height z_o and displacement thickness d, in neutral case, from:

$$\bar{u} = \frac{u_*}{K}\,\ell n\,\frac{z-d}{z_o} \qquad \text{(A-13)}$$

Using the same d, one can then determine the equivalent roughness height for heat and species, z_{o_θ} and z_{o_c} from:

$$\bar{\theta} = \frac{\theta_*}{K} \ln \frac{z - d}{z_{o_\theta}}$$

$$C = \frac{C_*}{K} \ln \frac{z - d}{z_{o_C}} \qquad \text{(A-14)}$$

Under strong stability conditions, the simple logarithmic relations (A-13) and (A-14) no longer hold and z_o and d have to be determined from Eq. 3-17.

Appendix B

SOME OTHER FACTORS WHICH CAN INFLUENCE FINE PARTICULATE DEPOSITION

The deposition model discussed in the main body of this report simulates the transport of fine particulates by 3 mechanisms across the thin, relatively laminar, sublayer next to a surface. These 3 mechanisms, Brownian diffusion, turbulent inertial impaction, and gravitational settling, should be the primary means. But other mechanisms may, under certain circumstances be important or even dominant. The purpose of this appendix is to estimate when some of these mechanisms need to be considered.

ELECTRICAL MIGRATION

The mobility of a charged particle in an electric field, E, is given by (36)

$$V_e = \frac{n_e e E}{3\pi\mu d_p} \qquad \text{(B-1)}$$

when n_e is the number of units of electronic charge e which the particle carries. For the standard atmospheric electric field of approximately 1 volt/meter this leads to a velocity of approximately 10^{-6} cm/sec for a particle with a 0.1 μm-diameter and a charge of 10 electrons. This is approximately 2 orders of magnitude below the gravitational settling velocity. Thus it appears that special circumstances such as much stronger electric fields (The normal surface field increases several orders of magnitude in the vicinity of thunderstorms.) and/or large charges on the particles are required for this mechanism to be important.

PARTICLE SIZE EVOLUTION

As evidenced by Equations 4-8 and 4-10, particle deposition is a strong function of particle size. In field experiments the exact particle size distribution is seldom known. Added to this uncertainty, there is the possibility that the size distribution can undergo considerable evolution within the canopy.

Numerous investigators have shown that sulfate aerosol size distributions depend strongly on relative humidity, particularly in the neighborhood of 100% R.H. A 10% increase in R.H. from 90% to 100% can increase the equilibrium radius of a NH_4HSO_4 aerosol by an order of magnitude, Fitzgerald (44). Thus the fact that the relative humidity varies from 100% within the leaf stomata to ambient conditions above the canopy can make the particle subject to considerable size evolution within the canopy.

Another mechanism possibly responsible for particle size distribution variations within the canopy is coagulation due to turbulent shear. Friedlander (36) estimates the reduction of the number density of particles of a prescribed density with time due to coagulation in a turbulent flow to be

$$N = N(o) \exp\left[- \frac{2}{3} d_p^3 N \left(\frac{\varepsilon d}{\nu}\right)^{\frac{1}{2}} t \right] \qquad \text{(B-2)}$$

For 1 μm-diameter particles with an initial concentration of 10^5 cm^{-3} in the presence of a high turbulent dissipation of 10^6 cm^2/sec^3 (corresponding to $q \simeq 2$ m/sec and $\Lambda = 1$ cm) the concentration will be reduced by a factor of 2 in approximately 10 minutes. If we assumed that the larger coagulated particles deposit on the canopy surface then this coagulation rate could be converted into a deposition rate by

$$V_{d_{(coagulation)}} \approx \frac{h}{N} \frac{dN}{dt} \approx \frac{2}{3} d_p^3 \left(\frac{\varepsilon d}{\nu}\right)^{\frac{1}{2}} Nh \qquad \text{(B-3)}$$

For our previous numerical example with $h = 10$ m this gives

$$V_d \approx 0.17 \text{ cm/sec} \qquad \text{(B-4)}$$

Thus under conditions of high concentration and strong turbulence, coagulation can play a significant role in particle deposition.

DIFFUSIOPHORESIS AND THERMOPHORESIS

Under some conditions the transport of heat or of another species between the surface and air can have an influence on the deposition of fine particles to that surface. In marked contrast to Brownian diffusion and inertial impaction, diffusiophoresis and thermophoresis are nearly independent of particle size. Therefore they

are likely to exhibit the strongest influence on particles in the size range from 0.1 to 1.0 μm-diameter where Figure 4-2 shows v_d to be a minimum.

Where another species (denoted here by subscript 2) is diffusing toward the surface a drift velocity of the medium is set up which can help carry the particles across the laminar sublayer adjacent to the surface. The incremental deposition due to this mechanism is given approximately by (45)

$$\Delta V_{d_{Diffusiophoretic}} = V_{d_2} \rho_2/\rho_{air} \tag{B-5}$$

This contribution may be ratioed to that due to Brownian motion. This ratio may be written as

$$\frac{\Delta V_{d_{Diff}}}{V_{d_{Brownian}}} = \frac{\rho_2}{\rho_{air}} \frac{D_2 \partial C_2/\partial n}{D_B \partial C_p/\partial n} \frac{C_p}{C_2} \tag{B-6}$$

$$\approx \frac{\rho_2}{\rho_{air}} \left(\frac{D_2}{D_B}\right)^{2/3} \left(1 - \frac{C_{2S}}{C_{2\infty}}\right) \tag{B-7}$$

In the case of moist air passing over a colder surface the 3 factors on the right hand side of Eq. B-3 may be estimated to be respectively $\rho_2/\rho_{air} \approx 0.01$, $(D_2/D_B)^{2/3} \approx 4 \times 10^3$ (for 0.5 μm-diameter particles), $(1 - C_{2S}/C_{2\infty}) \approx 0.1$ so that diffusiophoresis would dominate. Of course, in this case there would be an exchange of heat between the air and the surface.

The incremental deposition due to thermophoresis may be written as, whenever the ratio of the particle diameter to the mean-free path in air is $\lesssim 5$, following Friedlander (36):

$$\Delta V_{d_{Thermo}} = 0.5 \frac{\nu}{T} \frac{\partial T}{\partial n} \tag{B-8}$$

The ratio of this incremental deposition to that due to Brownian diffusion may be written as

$$\frac{\Delta V_{d_{Thermo}}}{V_{d_{Brownian}}} \approx 0.5 \frac{\nu}{D_B} \left(\frac{D_B}{\kappa}\right)^{1/3} \frac{\Delta T}{300} \qquad \text{(B-9)}$$

For a 0.5°C difference between the surface and the air above the sublayer this ratio would be ≈3.3. Thus thermophoresis can exceed Brownian diffusion when relatively modest temperature differences exist. Temperature differences between the air and the leaf depend principally upon net thermal radiation to the surface, the relative humidity of the air and the moisture content of the leaf. From Figures 13 and 14 in the review article by Jarvis, James, and Landsberg (46) it appears that even in the day time when the solar radiation forces the top layer of the canopy to have leaf temperatures exceeding air temperatures, the increment may be reversed in the lower portions of the canopy.

A detailed treatment of the contributions of thermophoresis and diffusiophoresis to deposition would require an accounting of the radiation exchange and the water balance within the canopy. This is beyond the scope of the present report.